Oncometabolite D-2-hydroxyglutarate - dependent metabolic reprogramming induces skeletal muscle atrophy during cancer cachexia

Quanjun Yang
Shanghai Jiao Tong University Affiliated Sixth People's Hospital https://orcid.org/0000-0003-0279-8784

Juan Hao
Department of Endocrinology, Shanghai Traditional Chinese Medicine-Integrated Hospital, Shanghai University of Traditional Chinese Medicine, 230 Baoding Road, Shanghai 200082, China

Hong Zhang
Department of Pharmacy, Shanghai Jiao Tong University Affiliated Sixth People's Hospital, 600 Yishan Road, Shanghai 200233, China

Mengyi Chi
Department of Pharmacy, Shanghai Jiao Tong University Affiliated Sixth People's Hospital, 600 Yishan Road, Shanghai 200233, China

Yaxian Wang
Department of Pharmacy, Shanghai Jiao Tong University Affiliated Sixth People's Hospital, 600 Yishan Road, Shanghai 200233, China

Yu Li
School of Pharmacy, Second Military Medical University, 325 Guohe Road, Shanghai, 200433, China.

Jinlu Huang
Department of Pharmacy, Shanghai Jiao Tong University Affiliated Sixth People's Hospital, 600 Yishan Road, Shanghai 200233, China

Lili Wan
Department of Pharmacy, Shanghai Jiao Tong University Affiliated Sixth People's Hospital, 600 Yishan Road, Shanghai 200233, China

Rong Xu
Department of Pharmacy, Shanghai Jiao Tong University Affiliated Sixth People's Hospital, 600 Yishan Road, Shanghai 200233, China

Xincai Zhao
Department of Pharmacy, Shanghai Jiao Tong University Affiliated Sixth People's Hospital, 600 Yishan Road, Shanghai 200233, China

Bo Xin

Department of Pharmacy, Shanghai Jiao Tong University Affiliated Sixth People's Hospital, 600 Yishan Road, Shanghai 200233, China

Xipeng Sun

Department of Pharmacy, Shanghai Jiao Tong University Affiliated Sixth People's Hospital, 600 Yishan Road, Shanghai 200233, China

Shumin Zhou

Department of Bone Oncology, Shanghai Jiao Tong University, affiliated Sixth People's Hospital Shanghai P. R. China.

Dongdong Chen

Department of Bone Oncology, Shanghai Jiao Tong University, affiliated Sixth People's Hospital Shanghai P. R. China.

Ting Yuan

Department of Bone Oncology, Shanghai Jiao Tong University, affiliated Sixth People's Hospital Shanghai P. R. China.

Jun Ding

Department of Bone Oncology, Shanghai Jiao Tong University, affiliated Sixth People's Hospital Shanghai P. R. China.

Shuier Zhen

Department of Oncology, Shanghai Jiao Tong University Affiliated Sixth People's Hospital, 600 Yishan Road, Shanghai 200233, China

Cheng Guo (guopharm@126.com)

Department of Pharmacy, Shanghai Jiao Tong University Affiliated Sixth People's Hospital, 600 Yishan Road, Shanghai 200233, China

---

Article

Keywords: IDH1, Oncometabolites, D-2-hydroxyglutarate, Cancer cachexia, Skeletal muscle

Posted Date: January 27th, 2022

DOI: https://doi.org/10.21203/rs.3.rs-1246702/v1

Abstract

Cancer cachexia is characterized by weight loss and skeletal muscle wasting. Based on the up-regulation of catabolism and down-regulation of anabolism, cachexia-associated metabolites and oncometabolites can accumulate in cancer patients. This study focused on genetic mutations-mediated metabolic reprogramming on cancer cachexia progression by screening for active metabolites and examined their direct effect on muscle atrophy. A total of 157 cachexia-associated metabolites and oncometabolites were selected based on literature collation, and 19 metabolites were screened with *in vitro* myotube differentiation model. D-2-hydroxyglutarate (D2HG) treatment led to a shorter myotube width and increased mRNA expression of E3 ubiquitin ligases *Trim63* and *Fbxo32*, as well as distinct transcriptional and metabolic changes. Then, we collected 149 cancer patients and confirmed Isocitrate Dehydrogenase 1 (IDH1) mutation in 19 patients with higher D2HG than non-mutational patients. Moreover, 8 cancer patients with IDH1 mutation and cachexia syndrome had higher D2HG. Mutated IDH1 (R132H) in the CT26 cancer cells accelerated cachexia progression (cachexia first occurred at DPI 17 in mice bearing wild-type CT26 tumor vs DPI 22 with mutational IDH1 CT26 tumor) and worsened the overall survival in the murine cancer cachexia model. E3 ligase *Trim63* and *Fbxo32* were increased by 2.3 and 1.4 times in muscle gastrocnemius of mice bearing CT26 tumor, while mice bearing CT26 tumor with mutational IDH1 increased 3.4 and 2.3 times respectively. Furthermore, overexpressed D-2-hydroxyglutarate dehydrogenase (D2hgdh) in well-differentiated myotubes alleviated 93μM D2HG induced shorter myotube width and upregulated E3 ligases. Transcriptomics and metabolomics revealed a distinct D2HG induced metabolic disequilibrium. Additionally, IDH1 inhibitor ivosidenib treatment delayed the progression of cancer cachexia in murine cancer model bearing CT26 colon carcinoma and GL261 glioma cancer cells. In the cachexia model of mice bearing CT26 tumor, ivosidenib decreased 58.5% serum D2HG concentration, preserved 15.1% muscle gastrocnemius mass and 11.9% lean body weight, improved 35.6% area of muscle gastrocnemius, and inhibited the unregulated mRNA expression of *Ube2d1, Trim63* and *Fbxo32*, when compared with NTC treated mice bearing CT26 tumor with IDH1 mutation. These results indicated the contribution of IDH1 mutation in mediating excessive D2HG accumulation in cancer cachexia progression and highlighted the possibility of individualized treatment for patients with cancer cachexia with an IDH1 mutation.

Introduction

Cancer cachexia is a multifactorial wasting syndrome characterized by progressive weight loss and persistent erosion of host body cell mass in response to a malignant growth [1,2]. Cancer cachexia is found in 50%-80% of cancer patients and is an independent predictor of poor prognosis [3]. Moreover, cachexia is associated with reduced treatment tolerance, therapeutic response, quality of life, and short survival. The ongoing loss of skeletal muscle mass contributes to progressive weight loss. Animal experiments suggested that maintaining skeletal muscle mass delays the process of cachexia and prolongs survival [4,5]. Currently, few treatments are available for preserving skeletal muscle mass as a treatment for

cachexia. Clinical evidence showed some types of solid cancer appear to have predisposition to induce cachexia [6].

The ongoing loss of skeletal muscle mainly occurs due to increased catabolism and decreased anabolism [1]. Metabolic reprogramming is common in cancer patients [7]. Multiple metabolites and metabolic pathway changes have been observed in cancer patients with cachexia [8–11]. Metabolic byproducts accumulate due to the excessive growth of the host's tumor and a dysfunctional metabolism. Studies have found genome instability and gene mutations also contribute to cancer-cachexia's metabolic reprogramming by regulating gene expression[12].

These altered metabolites not only accumulated through limited metabolic disposal capacity of cachexia, but also displayed extensive pathological and physiological functions. It was known oncometabolites contribute to tumorigenesis, angiogenesis, progression, and metastasis [13]. Still, little is known about whether genetic mutations mediated metabolic reprogramming can influence cancer cachexia initiation, progression, and treatment. For example, oncometabolite D2-hydroxyglutarate (D2HG) was produced by mutated isocitrate dehydrogenase (IDH)1/2. IDH1 mutation is found in various cancer types. D2HG is specifically elevated in cancer patients, including glioma, chondrosarcoma, acute myeloid leukemia, intrahepatic bile-duct cancer, and angioimmunoblastic T-cell lymphoma [12,14–19]. It was reported that D2HG was associated with myopathy [12,20]. However, the role of these cancer related metabolites on muscle metabolism remains unknown.

The present study examined the cancer related metabolites in cachexia development by screening for active metabolites and examining their effect on muscle atrophy. The effect of metabolites mediated muscle wasting was confirmed through mutation of oncogene and high metabolites treatment. Furthermore, downstream metabolic enzyme gene was over-expressed in *in vitro* experiment to reveal the mechanism, and enzyme inhibitor was used in *in vivo* experiments for pharmacodynamic research of cancer cachexia individualized treatment.

Results

The oncometabolites D2HG and fumarate induce muscle atrophy

After consulting published articles [8–11], we listed cancer cachexia-related metabolites, identifying 157 cachexia-related metabolites (Table S1). A total of 66 common metabolites were selected after excluding metabolites that changed in only one project. The metabolites were matched with the Human Metabolome Database (www.hmdb.ca) and the function annotations were included. Based on muscle-related functional annotation and accessibility of these metabolites, nineteen candidate metabolites were selected for the *in vitro* experiment (Fig. 1A, Table S2). The concentrations of these metabolites were listed based on reference (Table S2).

Well-differentiated myotubes were treated with these metabolites for *in vitro* screening, and myotubes diameters were measured (Fig. 1B-C). Fumarate (Fum), lactate, D2HG, pyruvate, adenosine, inosine, carnosine, phenylacetate, 1-methylhistidine, 3-methylhistidine, 4-hydroxyproline, and creatine induced different degrees of myotubes atrophy. To confirm the effect of metabolites mediated muscle wasting, we used the widely used *in vitro* muscle atrophy system and used mRNA expression of *Trim63* and *Fbxo32* upregulation as the index of muscle proteolysis [21]. When well-differentiated myotubes were treated with these 19 metabolites for 48 hours, succinate, fumarate, D2HG, 1-methylhistidine, 3-methylhistidine, and 4-hydroxyproline treatment resulted in significantly increase of mRNA expression of *Trim63* and *Fbox32* (Fig. 1D-E).

Genome instability and gene mutations of cancer cells drive the gain or loss of certain enzyme functions. On the other hand, they exert pro-oncogenic capabilities through metabolic reprogramming [22]. We searched the oncogenes and common cancer-based genetic alterations in the database of CancerGenetics Web (http://www.cancerindex.org/geneweb/), Cancer Gene Census(https://cancer.sanger.ac.uk/census), oncogene database (http://ongene.bioinfo-minzhao.org/), and database of Mutational Signatures (https://cancer.sanger.ac.uk/cosmic). A total of 2739 genes were included in the database (Table S3). Genotype/phenotype/disease associations were input based on comprehensive biological context for OMICs data interpretation [23]. To screen the metabolites-related genes, 84 genes were selected based on the association of gene annotation and metabolism (Table S4). Next, we searched the association between these genes and metabolic phenotype. It was found SDH and IDH1 were related with metabolites fumarate and D2HG. Thus, we further investigated the IDH1-mediated D2HG accumulation and SDH-mediated fumarate (Fum) accumulation (Fig. 1F). We treated the C2C12 myotube with D2HG and Fum for 72 h and confirmed morphological changes. The total RNA was then extracted for transcriptome sequencing. Heatmaps showed distinct transcriptional characteristics after D2HG treatment based on fragments per kilobase of exon model per million mapped fragments (FPKM) (Fig. 1G). The Fum treatment and NTC groups showed similar transcriptional features. These results confirmed that D2HG-induced myotube wasting occurs through proteolysis and with distinct transcriptional characteristics.

IDH1 mutation mediates high concentrations of D2HG in cancer patients with cachexia and *in vivo* cachexia mice model

D2HG is produced by mutant IDH1 [15], an unique R132H/C/G mutation at rs121913500 (Fig S1A). We obtained the IDH1 mutation information from patients, and nineteen out of 149 cancer patients were confirmed as an IDH1 mutation with PCR sequencing (Table S5). Then serum D2HG levels were measured using high-performance liquid chromatography-tandem mass spectrometry. The serum D2HG levels were higher in IDH1-mutated patients compared to controls (Fig. 2A). This was consistent with previous studies that abnormally elevated levels of D2HG to millimolar per gram of tissue in patients with a single mutant copy of IDH1 [6]. We defined cancer cachexia as weight loss >5% in the past 6 months or weight loss >2% in the past 6 months and a body mass index <20 kg/m^2 [2]. Among 19 IDH1-mutated

patients, 8 had cancer cachexia. The serum levels of D2HG were higher in cancer cachexia patients compared to those stable-weight cancer patients (Fig. 2B).

Next, we evaluated the IDH1 genotype-related cancer phenotype based on the public biological information resources of the TCGA database. The average alteration frequency of IDH1 was 5% in all cancer types, and the most common alteration type was mutation (Table S6). Substitution of the arginine 132 by histidine (R132H) accounted for >80% of all IDH mutations. To evaluate the overall survival of IDH1 alteration on pan-cancer, a total of 10,802 patients from 32 studies with mutation data were included after excluding 10 overlapping patients. A total of 627 IDH1-altered patients showed poorer overall survival than the IDH1-unaltered cancer patients (Fig S1B). Though IDH mutations have a different prognostic value depending on the cancer type, we still noted the IDH1 mutation mediated poor survival in pan-cancer patients. Moreover, the transcripts per million in different cancers ranged from 20 to 200, and cancer patients were higher than control patients (Fig S1C). We thus tested the hypothesis that IDH1 mutation mediated D2DH accumulation contributed to cancer cachexia progression.

IDH1 mutation at the amino acid arginine 132 (R132) is unique since it is localized in the isozymes' substrate-binding site [14]. IDH1 catalyzes the oxidative decarboxylation of isocitrate to ketoglutarate with NADPH's concomitant production. When IDH1 mutation occur in R132H, it hindered the hydrophilic interactions between the arginine and both α-carboxylate, and thus mutated IDH1 has gained a function that converts keto-glutarate and NADPH into D2HG and NADP. Based on the mutation frequency, we imported R132H into a cancer cell and used an *in vivo* experiment to evaluate whether IDH1 mutation mediated D2HG accumulation during cancer cachexia progression (Fig. 2C). BALB/c mice bearing CT26.wt colon adenocarcinoma cells are the most commonly used cancer cachexia model [24]. We first cloned IDH1-R132H into the lentivirus plasmid pLV-EF1α-FLAG-IRES-Puro and produced pLV-EF1α-IDH1-R132H-FLAG-IRES-Puro lentiviruses, which were used to infect CT26 colon adenocarcinoma cells. The amplification and the protein expression of IDH1 R132H were confirmed by sequencing the cDNA and Western blot (Fig S2A, Fig S2B). No IDH1 protein changes were observed in the wild-type group, while there was a higher expression of IDH1-R132H protein in the IDH1-mutated group (Fig S2B). Consistent with protein expression, the mRNA expression of IDH1-R132H was found higher (Fig S2C). Then, 2 million CT26 cancer cells were subcutaneously transplanted into the right flanks of male mice. The survival of the mice bearing IDH1-mutated cancer was shorter than in control mice (Fig. 2D). Cachexia was defined as lean body weight (mice without transplanted tumor) loss of more than 5% from the lean body weight change curve. For the IDH1-R132H mutation cancer-bearing mice, cancer cachexia syndrome occurred at DPI 17, and the average lean body weight decreased by 5.4% (from 26.83+1.12 g to 25.45+0.98 g) (Fig. 2E). However, cachexia was observed at DPI 22 in the wild-type tumor group since there was a decrease in lean body weight, and the bodyweight was decreased by 5.0% (from 27.09±1.10 g to 25.81±1.23 g). These results implied that the mutation of IDH1 in CT26 cells could accelerate the growth of tumors and induce the wasting of body weight.

To reveal the contributor of lean body weight loss, we measured the mass of typical skeletal muscle. Compared with the control group, skeletal muscle gastrocnemius and tibialis anterior loss in mice bearing

IDH1-mutated cancer was 26.1% and 16.3%, respectively (Fig. 2F). Furthermore, the loss of muscle gastrocnemius was 10.6% between the IDH1-mutated cancer group and IDH-wt group. Since skeletal muscles account for about 40% of total body weight, skeletal muscle weight loss was the main contributor to body weight loss. From the histopathology results of the muscle gastrocnemius (Fig. 2G), IDH1-mutated in tumor resulted in a smaller cross-sectional area in muscle gastrocnemius compared to the control groups and non-mutation CT26 tumor-bearing cancer cachexia mice (Fig. 2H).

Next, we extracted total RNA from the muscle gastrocnemius and measured the expression of the E3 ligases. *Trim63* and *Fbxo32* expression were increased by 2.3 and 1.4 times in CT26-bearing cachexia mice without IDH1 mutation (Fig. 2I). In contrast, they were dramatically increased 3.4 and 2.3 times in muscle gastrocnemius from the CT26-bearing cancer cachexia mice with IDH1 mutation compared with controls, respectively. These results implied that the degradation of skeletal muscle protein was enhanced via ubiquitinated protein system. To reveal the mediator of IDH1R132H mutation in cancer, we measured the levels of total D2HG in serum and tumor tissue. D2HG was enriched in IDH1 mutation tumor and serum (Fig. 2J), which was consistent with clinical data revealing that IDH1 mutation at R132 resulted in a high concentration of D2HG and high cachexia frequency in cancer patients. These results confirmed that muscle atrophy's deterioration was mediated by the high concentration of D2HG in CT26 bearing mice with an IDH1 mutation.

D2HG induces proteolysis via up-regulation of the ubiquitinated protein system and metabolic reprogramming

An *ex vivo* analysis of D2HG on differentiated multi-nucleus myotubes was designed (Fig. 3A). We treated well-differentiated multi-nucleus myotubes with 93 μM D2HG for 5 days, after which immunofluorescence was performed to detect myosin heavy chain (Fig S3A). The average myotube diameter of the D2HG treatment group was smaller than the NTC group (Fig S3B). To confirm the effect of protein degradation, we treated well-differentiated multi-nucleus myotubes with D2HG for 5 days and extracted total RNA. The mRNA expressions of E3 ligases of *Trim63* and *Fbxo32* were increased by about 11.7 and 20.4 folds, respectively (Fig S3C). Moreover, the E2 ubiquitin-conjugating enzyme *Ube2d1* was also increased 2.8 folds (Fig S3D). These results indicated that the upregulated expression of UPP contributed to D2HG-induced muscle atrophy.

D2HG can regulate transcription and metabolic processes, such as glycolysis [22], lipogenesis, oxidative stress, and methylation of histone[12]. We analyzed the transcriptional change of D2HG induced muscle atrophy and found distinct transcriptional profiling (Fig. 3B). D2HG treatment resulted in 412 transcriptional alterations based on fold change at 2.0 and adjusted *q* at 0.05 (Table S7). To reveal the primary mechanism responsible for the catabolic pathway, over-representation analysis (ORA) was used to screen the different genes. ORA-based gene ontology (GO) enrichment showed altered molecular function, biological process, and cellular component based on up- or down-regulated genes (Fig. 3C). Extracellular matrix structural constituent, structural molecule activity, structural constituent of the cytoskeleton, oxidoreductase activity, acting on the CH-OH group of donors NAD or NADP as acceptor,

glutathione transferase activity, and NAD binding were the top molecular functions. Moreover, the biological process and cellular components, including muscle cell differentiation, muscle tissue development, muscle system process, and muscle contraction, were also disturbed after D2HG treatment (Fig S4). We confirmed the correlation between muscle structure and metabolism resulting from D2HG treatment in differentiated multi-nucleus myotubes based on the GO enrichment analysis.

To reveal the distinct metabolic process responsible for the D2HG treatment, we extracted and measured the selected metabolites from well-differentiated myotubes using a targeted metabolomics strategy. Seventy-one metabolites were included based on the metabolic pathway of KEGG and previously reported metabolites [8–11]. Heatmap showed a distinct separation of the D2HG treatment group (Fig. 3D). A Joint Pathway Analysis was then used to integrate the changed metabolites and genes (Fig. 3E). The most characteristic pathways included glutathione metabolism, hypertrophic cardiomyopathy, aminoacyl-tRNA biosynthesis, citrate cycle synthesis, and degradation of ketone bodies. The changed metabolites based on the KEGG metabolic pathway were constructed (Fig. 3F) and we found D2HG exerted metabolic pathway reprogramming to disturb the maintenance of metabolic homeostasis.

D2hgdh mediated catabolism reverse D2HG induced proteolysis

We then analyzed the catabolic pathway of D2HG and explored the effect of D2HG catabolism on the reversal of proteolysis and muscle atrophy. D2HG is catabolized by D2hgdh, a mitochondrial enzyme that encodes D-2hydroxyglutarate dehydrogenase. Mutation of this gene in humans has been associated with developmental delay, epilepsy, hypotonia, and dysmorphic features [25]. Since well-differentiated myotubes cannot catabolize D2HG, we cloned D2hgdh into C2C12 myoblasts and induced its differentiation to myotubes. Typical immunofluorescence of myosin heavy chain staining showed normal differentiation for D2hgdh overexpressed C2C12 myoblast induced with a differentiation medium. Yet, there were sloppy myotubes after D2HG treatment (Fig. 4A). The myotube diameter of the D2HG-treated group was shorter than normal myotubes, while D2hgdh overexpression reversed D2HG induced myotube atrophy (Fig. 4B). We then measured the relative levels of D2HG and keto-glutarate in the differentiated myotubes. D2HG treatment resulted in high levels of D2HG and low keto-glutarate (Fig. 4C). No differences were found in keto-glutarate, while the levels of D2HG were decreased, which implied that the overexpression of D2hgdh in myotubes catabolism D2HG. We also measured the mRNA expression of *Ube2d1, Trim63*, and *Fbxo32* (Fig. 4D-E). Still, D2HG induced high expression of *Ube2d1, Trim63*, and *Fbxo32*, while D2hgdh over-expressing myotube inhibited the up-regulation of mRNA expression of these genes after D2HG treatment.

To confirm the expression of D2hgdh and related metabolic enzymes, we measured the protein expression by Western blot (Fig. 4F). D2hgdh overexpression showed high expression of *D2hgdh, Hmgcr, Hsd17b7, Dhrs3*, and *Adh7*, but low expression of *Idh1*. Hmgcr is a rate-limiting enzyme for cholesterol synthesis regulated via a negative feedback mechanism mediated by sterols. Anti-HMGCR antibody-positive patients often showed autoimmune myopathy and resemble limb-girdle muscular dystrophy [26]. Hsd17b7 regulates fatty acid metabolism and testosterone synthesis. Testosterone has pronounced

effect on muscle protein synthesis and muscle mass enlargement, especially during rapid muscle cell growth. A higher expression level of Hsd17b7 was observed in broilers, which might result in a higher testosis required for early embryonic patterning[27]. Dhrs3 protein is required for early embryonic patterning and upregulation of Dhrs3 was associated with osteogenic differentiation[28]. Single nucleotide polymorphism in *Adh7* was associated with multiple system atrophy[29]. Interestingly, the D2hgdh over-expression myotubes reversed the effect of D2HG. These results indicated that D2hgdh over-expression could enhance the catabolism of metabolites D2HG and subtract its proteolysis effect.

D2hgdh reprogramming metabolism of D2HG involving in multiple processes

HPLC-MS-MS-based targeted metabolomics was used to cluster the samples and discrete metabolites (Fig. 4G). All four groups were categorized based on 60 metabolites, and 2HG levels were low in the NTC and D2hgdh groups. Myotubes overexpressing D2hgdh showed a similar metabolic profile as the NTC group. D2HG treatment groups showed distinct metabolic characteristics, which indicated that D2HG could indicate distinct metabolism change. Moreover, D2HG treated myotubes overexpression D2hgdh were clustered between the two groups, thus indicating that D2hgdh overexpression could resist D2HG induced proteolysis. To directly show the metabolic pathway, we drew the metabolic pathway and the relative concentration of metabolites (Fig S5). From the changed metabolites of two independent experiments, 12 were enriched, and 15 were simultaneously depleted (Fig. 4H and Table S8).

To further reveal the transcriptional features of the four groups, a heatmap was used to reveal the clustering profile as metabolomics (Fig. 4I). D2HG triggered distinct transcriptional characteristics since the heatmap was clustered far from the NTC group. D2hgdh overexpression could resist D2HG induced gene alterations. The overall differentially expressed genes profile of the four groups showed that D2HG upregulated 1340 genes and downregulated 786 genes, while myotube overexpressing D2hgdh showed 20 upregulated genes and 65 downregulated genes with fold change at 2 and padj at 0.05 (Fig. 4J). These implied that D2HG induced a wide range of gene transcriptional level changes, while myotube overexpressing D2hgdh showed subtle perturbation. This set of experiments also included D2HG-treated well-differentiated myotubes and control myotubes (Table S9). In addition, based on the repeatability assay, the Venn diagram revealed the distinct transcriptional alteration, showing that 37 genes were commonly upregulated, and 101 genes were downregulated after D2HG treatment (Fig. 4K and Table S9).

To reveal the distinct transcriptional and metabolic characteristics of D2hgdh and evaluate the reversal of D2HG-mediated metabolic reprogramming with D2ghdh over-expression, we used the paired comparison on D2hgdh overexpression myotubes. First, we compared D2ghdh overexpression in well-differentiated myotubes with control well-differentiated myotubes (Table S10). The volcano plot showed the changed genes resulting from D2ghdh overexpression in well-differentiated myotubes (Fig. 5A). The downstream metabolites 2HG were decreased, which was consistent with the theoretical metabolic trend (Fig. 5B). The joint pathway analysis revealed several pathways, such as CoA biosynthesis and glutathione metabolism (Fig. 5C). To reveal the direct effect of D2ghdh overexpression on well-differentiated myotubes, GO analysis was used to display the molecular function, biological process, and cellular component (Fig S6).

Microtubule motor activity, microtubule-binding, tubulin binding, fibronectin-binding, ATPase activity, cell adhesion molecule binding, and activin receptor binding were the top molecular function.

Next, we compared the transcriptional and metabolic features between D2HG-treated myotubes over-expressing D2ghdh and NTC treated myotubes overexpressing D2ghdh to evaluate the D2hgdh over-expression on alleviation D2HG induced proteolysis (Table S11). It was found 241 genes were up-regulated, and 306 were down-regulated after D2HG treatment (Fig. 5D). NADH, lactate, 3-Methylhistidine, carnitine, and 2-hydroxyglutarate were enriched, while NADPH, NAD, and creatinine were depleted. GO analysis revealed the molecular function of oxidoreductase activity, acting on the CH–NH group of donors as top pathway enrichment (Fig S7). Moreover, D2ghdh induced the biology process alteration, such as sterol biosynthetic process, organic hydroxy compound metabolic process, and Acetyl-CoA metabolic process.

Furthermore, D2HG-treated D2ghdh over-expressing myotubes and D2HG-treated control myotubes were also compared (Table S12). A total of 1356 genes were depleted, and 640 genes were enriched (Fig. 5E); ATP-dependent serine/threonine kinase regulator activity was the top molecular function (Fig S8).

To interpret the gene expression data from D2hgdh over-expression and D2HG treatment, Gene Set Enrichment Analysis (GSEA) was used. D2HG-treated well-differentiated myotubes over-expressing D2hgdh showed enriched proteasome accessory complex and SUMO transferase activity, as well as depleted positive regulation of stem cell differentiation (Fig. 5F). These function annotations confirmed the D2HG mediated enhanced proteolysis and attenuated muscle differentiation.

To show the commonality relationships, the changed genes (Table S13) and Venn diagrams were used. Fifty-five common enriched genes and 52 common depleted genes were found (Fig. 5G). Metabolomics showed a series of common metabolic profiling, including depletion of 12 metabolites and enrichment of 8 metabolites after D2hgdh overexpression in well-differentiated myotubes, and depletion of 15 metabolites and enrichment of 12 metabolites after D2HG treated myotubes over-expressing D2hgdh when compared with D2HG treated control myotubes (Table S14). Venn diagram showed 1 commonly enriched metabolite and 5 commonly depleted metabolites (Fig. 5H). D2hgdh over-expression showed decreased 2HG, as well as isocitrate, carnitine, Fum, and NADH. D2hgdh could catalyze the conversion of D2HG to keto-glutarate with the driver of NAD to NADH. It was interesting that D2HG treatment resulted in decreasing NADPH/NADP ratio and increasing NADH/NAD ratio. However, when D2hgdh was over-expressed in myotubes, it could release the effect of D2HG and rescue the exhaustion of NADPH by cycling the redox balances and metabolic homeostasis[30]. Excessive D2HG could induce dysfunction of well-differentiation myotubes, while D2hghd over-expression myotube could catalyze D2HG and take advantage of metabolic reprogramming to drive the cycle of redox balances and metabolic homeostasis (Fig. 5I).

Ivosidenib relieves *Idh1* mutation mediated exacerbated cancer cachexia

Ivosidenib is a selective inhibitor of IDH1 mutation that blocks the abnormal IDH1 protein and can reduce abnormal D2HG levels [31]. We evaluated the effect of ivosidenib on relieving IDH1 mutation exacerbated cancer cachexia in mice bearing CT26 tumor (Fig. 6A). From DPI 9 of palpable tumor, mice bearing CT26 tumor and mice bearing CT26 tumor with IDH1 mutation were intravenously administrated with 50mg/kg ivosidenib or PBS as NTC control every day for the following experimental period [31]. Mice bearing CT26 tumor with IDH1 mutation showed a worse survival compared to the control mice (Fig. 6B). After treatment with ivosidenib, the survival of mice bearing CT26 tumor did not significantly change, while it was prolonged the survival of mice bearing CT26 tumor with an IDH1 mutation. As for the tumor weight curve, there were no changes between the two groups that did not receive treatment. Yet, after treatment, the tumor weight of control mice did not significantly change, while it was decreased in CT26 tumor with an IDH1 mutation. Ivosidenib preserved lean body weight in the IDH1 mutation tumor and delayed the cancer cachexia progression since the occurrence of cancer cachexia was first found at DPI 25 (Fig. 6C). To verify that ivosetinib has an impact on cachexia directly, we compared the lean body weight with a similar tumor weight of 1.56g (tumor volume 3000mm^3) and found there was a significant preserve of lean body weight in ivosidenib treated mice bearing CT26 tumor with IDH1-mutation when compared with NTC treated mice bearing CT26 tumor with IDH1-mutation (Fig. 6D). Next, we measured the cross-sectional area of the muscle gastrocnemius (Fig. 6E), and found the IDH1 mutation group was smaller than the control (Fig. 6F). Ivosidenib treatment prevented muscle atrophy. The IDH1 mutation also led to decreases in muscle gastrocnemius weight, while ivosidenib reversed the loss of muscle gastrocnemius (Fig. 6G). The mRNA expression of *Trim63* and *Fbxo32* was consistent with the histopathological results (Fig S9). IDH1 mutation in CT26 tumor-bearing mice resulted in increased expression of *Ube2d1*, *Trim63*, and *Fbxo32*, while ivosidenib treatment inhibited the upregulation of UPP-related enzymes. Serum D2HG concentration was increased after IDH1 mutation, while it was decreased after treatment with ivosidenib (Fig. 6H). These results indicated D2HG was a mediator of muscle wasting. Inhibition of the production of D2HG through IDH1 mutation inhibitor ivosidenib or catabolism of D2HG through over-expression of D2HGDH may reverse D2HG induced muscle proteolysis and slow down cancer cachexia procession.

Since IDH1 mutation was commonly found in glioma. We also established an orthotopic tumor model of in vivo bearing GL261 glioma cells with IDH1-mut. It was found the import of mutational IDH1 into GL261 glioma tumor resulted in significant improvement in survival (Fig. 6I). Ivosidenib could prolong the survival of mice bearing GL261 glioma tumor with mutational IDH1, however, not change the survival of mice bearing wild type GL261 glioma tumor. The loss of body weight was observed and loss of body weight over 5% occurred at DPI 15 for the mice bearing wild type glioma tumor and IDH1 mutational glioma tumor (Fig. 6J). After ivosidenib treatment, the cachexia syndrome occurred at DPI 17 for the mice bearing wild type glioma tumor, while at DPI 20 for the mice bearing IDH1 mutational glioma tumor. Though no significant change in muscle weight was found (Fig S10A), there was a significant decrease in muscle area (Fig. 10S B-C). Ivosidenib treatment resulted in significant improvement of muscle area. Moreover, the expression of E3 ligases *Trim63* and *Fbxo32* were increased in the muscle of mice bearing IDH1 mutation glioma tumor, while alleviated after ivosidenib treatment (Fig S10D). Moreover, serum

D2HG concentration was increased after IDH1 mutation, while it was decreased after treatment with ivosidenib (Fig. 6K).

Discussion

For well-differentiated skeletal muscle, cancer induces a catabolic proteolysis response characterized by activation of protein-degradation pathways, mainly through the UPP [3]. The present study revealed that the oncometabolite D2HG induced protein degradation and muscle atrophy by activating the ubiquitinated proteasome system and metabolic reprogramming in cancer cachexia. Based on the *in vitro* experiment, D2HG treatment increased expression of UPP E3 ligases genes, decreased myotubes diameter, inhibited differentiation, induced distinct transcriptional and metabolic features. This was consistent with previous reported that D2HG was associated with myopathy [12,20]. Furthermore, the *in vivo* experiment showed that the IDH1 mutation in CT26 cancer resulted in high serum levels of D2HG, loss of lean body weight and skeletal muscle, and increased expression of E3 ligases. The overall metabolic mechanism of IDH1 mediated D2HG accumulation and its contribution to proteolysis and muscle wasting were showed in Fig. 7.

The oncometabolite D2HG can accumulate up to millimolar in cancer patients[6]. D2HG formation/degradation imbalance has been associated with specific cancer metabolism, redox homeostasis, immunosuppressive, genetics, and epigenetics effects [32]. In this study, high D2HG was found in the cancer cachexia group. Moreover, patients with IDH1 mutation had high D2HG levels. Based on TCGA datasets, patients with IDH1 mutation had poor survival. Wild-type IDH1 catalyzes the oxidative decarboxylation of isocitrate to □-ketoglutarate with the concomitant production of NADPH. Mutations in IDH1 can be detected in various types of cancer, especially in low-grade gliomas[18,19], cholangiocarcinoma [14], lung cancer [17], renal cancer [6], pancreatic adenocarcinoma [15], and gastrointestinal cancer [11]. However, IDHs mutations have a different prognostic value depending on the cancer type. Gliomas with IDH1 mutation accounts for the unfavorable prognostic effect of higher age[18,19], while there was no direct association in clinical outcome in intrahepatic cholangiocarcinoma patients with mutational IDH1[33]. Commonly, these solid cancers have a high incidence of cancer cachexia syndrome[3]. In this study, we cloned the cDNA of IDH1-R132H after the promoter of EF1α and produced a lentivirus to gain the function of IDH1-R132H in CT26 colon carcinoma cells and GL261 glioma cells. When the CT26 tumor cells with IDH1-R132H were transplanted in BALB/c mice, the overall survival was shorter, and the lean body weight decreased faster. Moreover, the cachexia occurred earlier in the presence of the IDH1 mutation. However, When the GL261 glioma cells with IDH1-R132H were transplanted in C57BL/6J mice, the survival was improved. There was no significant difference in body weight loss, and the occurrence of cachexia was similar. While IDH1 inhibitor ivosidenib could significantly improve survival.

The mechanism of cancer-induced loss of skeletal muscle mass is complex [1,3]. Many mediators, including inflammatory cytokines, chemokines, glucocorticoids, and metabolites, are elevated due to host

and cancer interaction [1]. These mediators are released and circulated to the skeletal muscle through the circulatory system. When these mediators act on skeletal muscles, they disturb substrate metabolism and cause function alteration. UPP activation was observed in the wasting muscles from multiple *in vitro* and *in vivo* experiments and was recognized as the key mechanism for muscle atrophy [3]. In the present study, D2HG treatment in well-differentiated myotubes directly led to short myotube diameter and upregulated E3 ligases and E2 ubiquitin-conjugating enzyme. The gain of function of IDH1 mutation in CT26 tumor also led to high D2HG concentration in circulation and upregulated E3 ligases in skeletal muscle. A GSEA of the transcriptional features revealed that D2HG treatment in well-differentiated myotubes resulted in enriched proteasome accessory complex and SUMO transferase activity and depleted positive regulation of stem cell differentiation. This study found that *Sema3c, Hoxb4, Tgfb2, Gata6, Nkx2-5, Ltbp3*, *Sox5*, and *Ptn* were depleted by D2HG. *Gata6* is required for cardiovascular development and myosin heavy chain gene expression [34]. *Nkx2-5* has RNA toxicity in myotonic muscular dystrophy [35]. The ectopic expression of *Ltbp-3* in mature mouse skeletal muscle increases fiber area and reduces myostatin activity [36]. *Ptn* is a heparin-binding growth factor that impairs muscle reinnervation and decreases cell density in muscle gastrocnemius injury [37]. Therefore, these factors could be mediators of the effects of D2HG. On the other hand, D2ghdh overexpression in D2HG-treated myotubes influenced the extracellular matrix, myosin complex, and spindle microtubule. Myosin is a motor protein that participates in the generation of mechanical force in myofibers. Muscle myosin molecules are heterohexamers composed of two myosin heavy chains and two myosin light chains [24]. Selective loss of myosin mainly contributed to the wasting of skeletal muscle during cancer cachexia via UPP, thus verifying that the high levels of D2HG induced muscle atrophy via UPP mediated proteolysis.

The transcriptome and metabolome's integrated analysis revealed the distinct effect of D2HG on well-differentiated myotubes through metabolic reprogramming. Accumulated D2HG impaired the function of myotubes and induced proteolysis through NADPH exhaustion. D2HG increased the NADH/NAD+ ratio while decreased the NADPH/NADP ratio. While D2hgdh over-expression in myotubes relieved D2HG induced increasing NADH/NAD+ ratio and decreasing NADPH/NADP ratio. D2hgdh is a mitochondrial enzyme that catalyzes the conversion of D2HG to keto-glutarate with the driver of NAD+ to NADH. When D2hgdh was over-expressed in myoblasts, the differentiation from myoblasts to myotubes was unaffected. The rescue of NADPH exhaustion after treatment of D2HG in the D2hgdh over-expressed myotubes indicated the reprogramming of redox homeostasis.

Metabolic changes in cancer are acknowledged as a possible therapeutic target. In this study, we inhibited the production of D2HG in tumor with IDH1 mutation using the selective IDH1 inhibitor ivosidenib. Our results showed that ivosidenib could delay the progression of cancer cachexia syndrome. Furthermore, ivosidenib preserves skeletal muscle mass by decreasing the expression of the E3 ligases *Trim63* and *Fbxo32*, as well as inhibiting the production of D2HG in tumor and serum.

Cancer cachexia is characterized by lean body weight loss and skeletal muscle atrophy. Refractory cachexia is a contraindication for multiple treatments and clinical trials. Though multiple cachexia

mediators were researched [1], genetic factors were ignored in the progression of cancer cachexia. Commonly, gene mutation or differential expression has not been recognized as directly responsible factor for proteolysis and cachexia symptoms. In the present study, cancer patients with IDH1 mutation had high levels of D2HG, which could exacerbate proteolysis and induce cancer cachexia. These results highlight the precision medicine of cancer cachexia and the comprehensive treatment of cancer patients.

Three limitations were worthy of further research. There are extensive metabolic abnormalities in cancer patients, and different cancer types have distinct metabolic profiles. Our experiment provided evidence that physiologically concentration D2HG induced proteolysis and muscle atrophy. It was worthy of attention for the contribution of other changed cancer metabolites on muscle metabolism and muscle wasting, such as succinate, fumarate, D2HG, 1-methylhistidine, 3-methylhistidine, and 4-hydroxyproline, at physiologically concentration. Another limitation of this study was its genetic contribution to the development of cancer cachexia. IDH1 mutation resulted in significantly short survival in subcutaneous tumor model with CT26 colon carcinoma tumor, and significantly prolonged survival in orthotopic tumor model with GL261 glioma tumor. However, the treatment of ivosidenib in both models showed prolonged survival and delayed weight loss. After analyzing the metabolites, we concluded the direct contribution of oncometabolite D2HG on proteolysis and muscle wasting. Third, there was a bias for the endpoint of the murine cancer cachexia model since mice were individually culled when reaching the humane endpoint that our veterinarian marked the animal sick. When we got the significantly different experiment endpoint of the changed lean body weight, all the alive mice were euthanized. Future studies are needed to further examine the potential of ivosidenib for individualized anti-cachexia effect in cancer patients with an IDH1 mutation.

In conclusion, mutational IDH1 mediated D2HG accumulation leads to metabolic reprogramming and distinct transcriptional features in differentiated myotubes. Catabolizing D2HG by the overexpression of D2hghd and inhibiting the production of D2HG using the IDH1 mutation inhibitor ivosidenib could reverse D2HG-mediated proteolysis and muscle atrophy. These results revealed the possibility of individualized treatment of cancer cachexia in patients with an IDH1 mutation.

Materials And Methods

Study approval and sample collection

Ethics approval

was obtained from the Health Research Ethics Board at Shanghai Jiao Tong University Affiliated Sixth People's Hospital. Patients were recruited between July 2013 and May 2020. All participants provided written informed consent. Sample identification numbers were used as unique, anonymous identifiers that were independent of true identifiers of each patient. Based on the diagnostic criteria from the international consensus [2], cancer patients with and without cachexia were recruited. Cancer patients with cachexia were included according to the following criteria: weight loss >5% over the past 6 months, or

weight loss >2% over the past 6 months, and a body mass index (BMI) <20 kg/m^2. Weight-stable cancer patients were those with BMI <25 kg/m^2 but no marked weight change during the previous year. Age, height, weight, cancer biomarkers, and biochemical biomarkers were obtained from the patients' laboratory reports, either from the date of diagnosis or the date closest to diagnosis. To exclude the effect of chemotherapy on the production of D2HG, the cachectic and weight-stable cancer patients were free for chemotherapy at least 21 days when the samples were collected. The exclusion criteria were: kidney or liver failure; acquired immunodeficiency syndrome; inflammatory bowel disease; systemic infection.

Tissue genotyping

The IDH1 genotype was determined using Sanger sequencing. Formalin-fixed and paraffin-embedded tumor specimens were retrieved to extract DNA using QIAamp DSP DNA FFPE Tissue Kit (Qiagen, Venlo, Netherlands). PCR amplification was performed in a 20-μl reaction mixture containing 200 ng of DNA, 0.6 μL of forward and reverse primers, 10 μl of 2× PCR Master Mix buffer (Qiagen, Venlo, The Netherlands) and RNase-free water. PCR reaction was performed at 96°C for 30 s, followed by 35 cycles of denaturation at 96°C for 10 s, annealing at 55°C for 10 s, and extension at 72°C for 20 s. The products were sequencing and the results were aligned to identify the mutation of IDH1.

Serum D2HG determination

Sera D2HG levels were determined with a 6490 Triple Quadrupole LC/MS [12]. Briefly, 200 μL of thawed serum was mixed with 800 μL of acetonitrile and centrifuged at room temperature (24°C) for 10 min at 10,000 rpm. The supernatants were then transferred to polypropylene tubes and evaporated under a vacuum. The residues were reconstituted with 50 μL of 90% methanol in water (v/v), and 10 μL was injected into an Agilent 6490 Triple Quadrupole LC/MS System. Chromatographic separation was achieved through a Chirex 3126 (D)-penicillamine, LC Column (150 × 4.6 mm, Phenomenex, Torrance, CA, USA). Data collection, peak integration, and processing were performed with the MassHunter Software (Agilent Technologies, Santa Clara, CA, USA). Reagents of MS-grade were used for extractions. Pure D2HG was used as a standard to calculate the D2HG levels.

Cell culture

All cell lines were verified to be mycoplasma-free. The CT26.wt colon carcinoma cells (ATCC; Manassas, VA, USA) and GL261 glioma cells were cultured in Dulbecco's Modified Eagle Medium (DMEM) supplemented with 10% fetal bovine serum and penicillin-streptomycin (100 U/mL and 100 mg/mL, respectively) in a humidified atmosphere containing 5%CO_2/95% air at 37ºC.

Murine C2C12 myoblasts were obtained from the Cell Bank of the Typical Culture Collection Committee of the Chinese Academy of Sciences. Low-passage C2C12 myoblasts were first cultured in growth DMEM medium supplemented with 10% fetal bovine serum and penicillin-streptomycin (100 U/mL and 100 mg/mL, respectively) in a humidified atmosphere containing 5%CO_2 air at 37ºC. C2C12 myoblasts (<15 passages) were induced by replacing the culture medium with fusion medium (DMEM with 2% horse

serum and 1% penicillin/streptomycin). When the C2C12 myoblasts in the growth medium reached about 80%-90% confluence, a substantial volume of the medium was added, and incubation was continued for 4 days. The differentiation medium was changed every 3-4 days after myotubes were formed. Cell culture-based experiments were performed in independent triplicates.

Ex vivo myotube wasting model and metabolites treatment

For the *in vitro* myotube wasting model, well-differentiated myotubes exposed to 100 μM dexamethasone were positively controlled [38]. Metabolites were added to the differentiation medium to induce muscle atrophy. These media were used for the culture of the myotubes for >2 days.

Immunofluorescence

Well-differentiated myotubes from different groups were fixed with 4% formaldehyde for 20 min at room temperature. The myotubes were washed with PBST and blocked in 5% bovine serum albumin (dissolved in PBST) for 60 min at 37°C. The cells were incubated with primary anti-myosin heavy chain antibodies (1:200) overnight at 4°C. After washing the cells three times with PBST and incubating with the corresponding Alexa Fluor 488-conjugated secondary antibody for 60 min at 37°C, the cells were washed three times with PBST for 5 min. The nuclei were stained with DAPI for 3 min, followed by three washes with PBST. An anti-fluorescence quenching agent was then added, and fluorescence images were obtained using a fluorescence microscope. IgG controls validated the specificity of myosin heavy chain primary antibodies by only fluorescent secondary antibody staining. Each myotube width was measured at the widest crosscut direction, and each myotube was measured at three different regions (the average value was the width). Each group contained 3 biological duplications and at least 80 myotubes. ImageJ was used to quantify the myotube width and area.

Overexpression of D2hgdh in C2C12 myoblast using a lentivirus

The cDNA of IDH1 with the R132H mutation (NM_005896.2) was amplified with PCR (primers are shown in Table S15). The plasmid pLV-EF1α-FLAG-IRES-Puro was digested with EcoR1 and BamH1. The lentivirus plasmid pLV-EF1α-IDH1-R132H-FLAG-IRES-Puro was produced through Gibson assembly. The resulting plasmid was sequenced to check that the insert was properly inserted. D2hgdh over-expression lentivirus pLV-EF1α-D2hgdh-FLAG-IRES-Puro was also cloned. The lentiviruses were produced in low-passage HEK293 cells. About 2 h before transfection, complete DMEM media were replaced with 13 mL of pre-warmed Opti-MEM medium (Invitrogen Inc., Carlsbad, CA, USA). For each 15-cm plate, 450 μL of Opti-MEM was mixed with 20 μg lentiviral transfer plasmid, 15 μg psPAX2 packaging plasmid, 10 μg pMD2.G envelope plasmid, and 130 μl polyethyleneimine. The mixture was incubated for 15 min at room temperature and added to cells. After 6-12h, the Opti-MEM media was replaced with 20 mL of pre-warmed complete DMEM media. Viral supernatant was collected at 48 h and 72 h post-transfection. Cell debris was removed by centrifugation (5 min at 2000 rpm). Lentiviruses were concentrated using AmiconUltra 100 kD ultrafiltration centrifugal tube (Millipore) and stored at -80°C. To produce D2hgdh over-expressed C2C12 myoblasts, 0.2 ml of concentrated lentiviruses was added into low-passage C2C12 myoblasts at

5×10^4 cells per well in 24-well plates. The myoblasts were cultured for 16 h. The D2hgdh over-expressing myoblasts were selected using 1 μg/ml antibiotics for 7 days.

Western blot

Well-differentiated myotubes were homogenized and solubilized in ice-cold RIPA buffer containing protease inhibitors. After incubation on ice for 30 min, the protein supernatant was collected after centrifuging at 12,000 ·g and 4°C for 15 min. The protein concentration was measured using a BCA Protein Assay Kit BCA assay kit (Thermo Fisher Scientific, Waltham, MA, USA). The same amounts of proteins were mixed with 5· loading buffer and boiled for 5 min. Then, 20 mg of protein was loaded onto a 10% SDS-polyacrylamide. The proteins were separated and transferred on PVDF membranes. The membranes were blocked at room temperature for 1 h using 3% bovine serum albumin in TBST buffer. The membranes were then incubated with primary antibody (diluted with 3% bovine serum albumin in TBST buffer at 1:1000) at 4°C overnight and then washed three times with TBST. Next, the membranes were incubated with diluted secondary antibody (horseradish peroxidase (HRP)-conjugated secondary antibodies diluted with TBST buffer at 1:3000) at room temperature for 1 h and washed three times with TBST. The protein expression was detected using a chemiluminescence imaging system. The protein expression was quantified using the ImageJ program. Equal distribution of protein loading was verified by probing the blots with an anti-GAPDH antibody.

Total RNA extraction and quantitative PCR

Total RNA was extracted from different tissues using Trizol. The first-strand cDNA from total RNA preparations was synthesized with M-Mlv Reverse transcriptase after normalizing with nuclease-free water. Quantitative qPCR was performed by adding SYBR Premix Ex Taq II and designated probes of interesting genes with synthetic primers (Table S15). All samples were tested in triplicates. GAPDH was used as an internal positive control. Relative mRNA calculations were analyzed using the $2^{-\Delta\Delta CT}$ method.

mRNA seq

The total RNA of each group was used for the mRNA library preparation following a standard RNA extraction protocol. After the first strand reaction buffer and random primer mix, 1000 ng of total RNA was fragmented and processed for first-strand cDNA synthesis and second-strand cDNA synthesis. The double-stranded cDNA was purified, and adaptor ligation was performed. The samples were then multiplexed using barcoded primers. The PCR conditions were one cycle of 30 s at 98°C, followed by 11 cycles of 10 s at 98°C, 75 s at 65°C, and finally with 5 min incubation at 65°C. The adaptor-ligated library was purified and sent for quality assessment. In the library's case of good quality, the libraries were sequenced using Novaseq systems (Illumina, Inc., San Diego, CA, USA). The raw sequencing files were available via SRA with metadata of mRNA-seq (Table S16). Each sample was run in triplicate. The RNA-seq data were deposited in the NCBI Sequence Read Archive under accession number: SUB8925446 and SUB8927518.

mRNA-seq data analysis

Raw FASTQ files from RNA-sequencing were analyzed for transcriptional quantification using QianTang Biotech Co., Ltd (Suzhou, China). Transcriptome references were obtained from Ensembl. To estimate transcript abundances, we applied HISAT to the aligned reads and summarized transcript abundances into gene-level expression levels. StringTie was used for transcript prediction, and Bowtie2 was used to align sequencing reads to long reference sequences. Packages of DEseq2, EBseq, NOIseq, and PossionDis were used to identify up- and down-regulated genes. KEGG and GO analysis were done with a cluster Profiler. GSEA was performed using the Java application from the Broad Institute. The full gene set from the differential gene expression analysis was ranked by “beta” value and then used as an input for GSEA pre-ranked analysis with database reference C5 Gene Ontology - Biological Process (GO-BP). Visualization, including volcano plots, bar plots, and Venn diagrams, were performed using standard R packages ggplot2. Enriched and depleted genes from the differential gene expression analysis were defined with an adjusted *p*-value cutoff of 0.05 and fold change as 2.0.

Metabolomics and data analysis

Each sample was tested in five duplicates, each containing 2 million living cells. To extract the intracellular metabolites, the cells were washed with PBS twice and resuspended in 800 µL of 80% (vol/vol) methanol (precooled to -80^{o}C) on dry ice for 30 min. The tubes were incubated on ice for 20 min and centrifuged at 15,000 g for 15 min at 4^{o}C. The metabolite-containing supernatant was then transferred to a new tube on dry ice and centrifuged again (see above). Next, the mixture was dried by Speedvac. The metabolites were dissolved with 80% (vol/vol) methanol, centrifuged at 18,000 ×g, and kept at -80°C until LC-MS analysis on an Agilent 6550 Q-TOF LC/MS System. The targeted metabolomics was analyzed with an Agilent 6490 Triple quadrupole LC/MS System. Liquid chromatography was optimized with the Kinetex 2.6-µm PS C18, LC column 150 × 2.1 mm (Phenomenex, Torrance, CA, USA). The eluents were A: 0.01% formic acid in HPLC grade water and B: 0.01% formic acid in acetonitrile. The gradient was set as follows: 0-2 min 5% B; 2-36 min 5-100% B; 36-40 min hold at 100% B and then returned to initial conditions for 2 min for column equilibration. The flow rate was set as 0.3 mL/min.

Multiple reaction monitoring was used for the qualitative and quantitative analysis of purified standards (Sigma, St. Louis, MO, USA). The features of spectra were extracted using Agilent Mass Hunter Qualitative Analysis Software (Version B 6.0.633.0). Each peak was checked, and the abundances of all metabolites were exported. The retention times of the standards were confirmed. Three normalization procedures, such as normalization by sum, log transformation, and auto-scaling, were used to compare individual features. Distance Measure was set as Euclidean, and the Clustering Algorithm was set as Ward. Finally, the metabolic flowchart functions were constructed with the software Pathvisio v3.3.0 based on the KEGG database. The integrated analysis of the changed metabolites and genes was performed with the Joint Pathway analysis module of MetaboAnalyst 5.0. Volcano plots were used to filter metabolites of interest with significant fold changes at 2.0 and statistical significance at 0.05 with the software MetaboAnalyst 5.0.

Multi-omics analysis

The differential expressed genes from the RNA sequencing analysis and differential represented metabolites were input for common pathway analysis using the MetaboAnalyst Portal. Default parameters were used, with hypergeometric test for enrichment analysis, Degree centrality for topology analysis, and gene-metabolite pathways for pathway databases. Pathways were considered statistically significant if the *p*-values were <0.05.

Cancer cachexia model of in vivo bearing CT26 cells with IDH1-mut

All animal studies were approved by the institutional Animal Welfare Committee at Shanghai Jiao Tong University Affiliated Sixth People Hospital, according to the government guidelines for animal manipulations in China. BALB/c mice bearing CT26 colon carcinoma tumor was a common mice model used to study cancer cachexia in vivo[39]. Cancer cachexia model bearing CT26 tumor with IDH1 mutation was established via the establishment of a positive clone of CT26 cells that expressed mutational IDH1. Briefly, we cloned IDH1-R132H into the lentivirus plasmid pLV-EF1α-FLAG-IRES-Puro and produced pLV-EF1α-IDH1-R132H-FLAG-IRES-Puro lentiviruses, which were used to infect CT26 colon adenocarcinoma cells. After selection through adding antibiotics, we got a positive clone of CT26 cells with mutational IDH1 (CT26-IDH1-mut cells). Then we verified the protein and mRNA expression of mutational IDH1 in the CT26 cancer cells. The CT26 cells with mutational IDH1 were then used to establish cancer cachexia model and pharmacology research. Male BALB/c mice (about 7 weeks), which were from Shanghai SLAC Laboratory Animal Co. Ltd (Shanghai, China), were housed in an environment with a constant temperature of 22 ± 1 ºC and relative humidity of 50 ± 1%, with free access to food and water. After acclimatization for one week, mice were divided into responsible groups, and each group had 10 mice. A cancer cachexia group received a subcutaneous injection of 100 μl cancer cells (1×10^6 cells) into the right flank to induce the cancer cachexia model, while an equal volume of vehicle phosphate-buffered saline (PBS) was subcutaneously injected into the right flanks of control mice. The tumors were palpable on day 9, and the mice without palpable tumors were excluded. Mice were grouped and intravenously administered with 50mg/kg ivosidenib or PBS as NTC control every day for the following experimental period. Tumor length and width were measured using a digital caliper every other day. The tumor weight (g) was calculated using the formula 0.52× tumor width (cm) × length (cm)2, and the lean body weight was calculated by subtracting the tumor weight from the total animal weight. The mice were euthanized by ethical criteria (veterinary authority-stipulated endpoint including loss of ~25% initial body mass). The blood was then collected into tubes, and the serum was prepared within 1 h. The tumors were dissected and weighed. The muscle gastrocnemius from both the hind legs was quickly removed and weighed. One half was snap frozen in liquid nitrogen, and the other half was □xed in 10% neutral buffered formalin.

Orthotopic tumor model of in vivo bearing GL261 cells with IDH1-mut

The GL261 cells with mutational IDH1 were then used to establish cancer model and pharmacology research. Briefly, GL261 glioma cells with mutational IDH1 were produced as previous methods using

lentiviruses. Male C57BL/6J mice (about 7 weeks), which were from Shanghai SLAC Laboratory Animal Co. Ltd (Shanghai, China), were anesthetized with a mixture of ketamine 80 mg/kg and xylazine 10 mg/kg. Then 3×10^5 GL261 cells with mutational IDH1 in 2 μl HBSS were implanted intracranially using a Stoelting stereotaxic apparatus (2.5 mm lateral to the bregma and 3.0 mm below the skull). Since day 7 of a palpable tumor, mice were grouped and intravenously administered with 50mg/kg ivosidenib or PBS as NTC control every day for the following experimental period. Mice were monitored daily and sacrificed at veterinary authority-stipulated endpoint (sick or loss of ~25% initial body mass). The muscle gastrocnemius from both the hind legs were quickly removed and weighed. One half was snap frozen in liquid nitrogen, and the other half was xed in 10% neutral buffered formalin. The blood was then collected into tubes, and the serum was prepared within 1 h.

Histopathology of muscle gastrocnemius

Transverse serial sections of muscle gastrocnemius were fixed with 4% paraformaldehyde in 0.2 M phosphate-buffered saline (PBS) for 5 min at room temperature, washed with PBS, and stained using hematoxylin and eosin (Sigma, St. Louis, MO, USA). Images of muscle gastrocnemius sections were recorded.

Metabolite extraction and quantitative determination of D2HG

Tumor tissues (10 mg) were extracted by grinding with liquid nitrogen, and tumor fragments were homogenized in 1000 μL of prechilled 80% HPLC-grade aqueous methanol. After centrifugation at 14,000 ×g for 15 min, the supernatants were transferred to polypropylene tubes and evaporated under vacuum. The residues were reconstituted with 50 μL of methanol-water (90%:10%; v/v), and 10 μL was injected into an Agilent 6490 Triple Quadrupole LC/MS System. Sera D2HG levels were determined using relative quantitative method.

Statistical analysis

Data were summarized using means and standard deviations (SD). Two-sided paired Student's t-tests were used for the analysis of two groups. One-way ANOVA analyses with Tukey post-hoc testing were performed for multiple comparisons. Survival data for mice were tested for statistical significance by the Kaplan–Meier curves with two-sided log-rank Mantel–Cox analysis. The relative expression was determined by comparing the treatment values to the control values after normalization to controls. Statistical significance was assessed using the GraphPad Prism software (****p<1e-4, ***p<2e-4, **p<2e-3, *p<0.033).

Declarations

Author contributions

QY, CG: designed and performed most of the experiments in the study. JH (Juan), RX, DC, TY, JD, SZ (Shuier): Clinical samples collection and analysis. YL, XZ: performed metabolites selection, metabolomics, and transcriptome analysis. HZ, MC, YW, SZ (Shumin): performed cell culture, sample preparation, and molecular biology experiment. QY, JH(Juan), MC, YW: performed the animal experiment. JH(Jinlu), BX, LW: performed data analysis and participated in technical advice. QY, JH, and CG: Manuscript preparation.

ACKNOWLEDGMENTS

The authors acknowledge the help of the Analysis and Testing Center of Shanghai Jiaotong University and Naval Medical University (metabolomics analysis and metabolites determination) and Qiantang Biotechnology (Suzhou) Co., Ltd (transcriptomics analysis).

Conflict of interest

All the authors declare that they have no conflict of interest.

FUNDING

This study was supported by the National Natural Science Foundation of China (No. 81872494, 81873042, 82074063 and 81803874), Excellent Young Medical Talent Training Program of Shanghai Municipal Health Commission (2018YQ19) and Shanghai Pujiang Talent Program (21PJ1411900).

Data and materials availability

All the data analyzed in the paper are presented in the paper and the Supplementary Materials. The RNA-seq data were deposited in the NCBI Sequence Read Archive under accession number: SUB8925446 and SUB8927518. Additional data related to this paper are available from the authors.

References

1. Baracos, V. E., Martin, L., Korc, M., Guttridge, D. C. & Fearon, K. C. H. Cancer-associated cachexia. Nat Rev Dis Primers **4**, 17105, doi:10.1038/nrdp.2017.105 (2018).
2. Fearon, K. *et al.* Definition and classification of cancer cachexia: an international consensus. Lancet Oncol **12**, 489–495, doi:10.1016/S1470-2045(10)70218-7 (2011).
3. Biswas, A. K. & Acharyya, S. Understanding cachexia in the context of metastatic progression. Nat Rev Cancer **20**, 274–284, doi:10.1038/s41568-020-0251-4 (2020).
4. Zhou, X. *et al.* Reversal of cancer cachexia and muscle wasting by ActRIIB antagonism leads to prolonged survival. Cell **142**, 531–543, doi:10.1016/j.cell.2010.07.011 (2010).
5. Parajuli, P. *et al.* Twist1 Activation in Muscle Progenitor Cells Causes Muscle Loss Akin to Cancer Cachexia. *Dev Cell* **45**, 712-725 e716, doi:10.1016/j.devcel.2018.05.026 (2018).

6. Yong, C., Stewart, G. D. & Frezza, C. Oncometabolites in renal cancer. Nature Reviews Nephrology **16**, 156–172 (2020).
7. Faubert, B., Solmonson, A. & DeBerardinis, R. J. Metabolic reprogramming and cancer progression. Science **368** (2020).
8. Boguszewicz, L. *et al.* NMR-based metabolomics in real-time monitoring of treatment induced toxicity and cachexia in head and neck cancer: a method for early detection of high risk patients. Metabolomics **15**, 110, doi:10.1007/s11306-019-1576-4 (2019).
9. Yang, Q. J. *et al.* Serum and urine metabolomics study reveals a distinct diagnostic model for cancer cachexia. J Cachexia Sarcopenia Muscle **9**, 71–85, doi:10.1002/jcsm.12246 (2018).
10. O'Connell, T. M. *et al.* Metabolomic analysis of cancer cachexia reveals distinct lipid and glucose alterations. Metabolomics **4**, 216 (2008).
11. Miller, J. *et al.* Plasma metabolomics identifies lipid and amino acid markers of weight loss in patients with upper gastrointestinal cancer. Cancers **11**, 1594 (2019).
12. Karlstaedt, A. *et al.* Autophagic signaling promotes systems-wide remodeling in skeletal muscle upon oncometabolic stress. *bioRxiv*, 2020.2010.2013.338202, doi:10.1101/2020.10.13.338202 (2021).
13. Williams, D. & Fingleton, B. Non-canonical roles for metabolic enzymes and intermediates in malignant progression and metastasis. Clin Exp Metastasis **36**, 211–224, doi:10.1007/s10585-019-09967-0 (2019).
14. Borger, D. R. *et al.* Frequent mutation of isocitrate dehydrogenase (IDH)1 and IDH2 in cholangiocarcinoma identified through broad-based tumor genotyping. Oncologist **17**, 72–79, doi:10.1634/theoncologist.2011-0386 (2012).
15. Brody, J. R. *et al.* Identification of a novel metabolic-related mutation (IDH1) in metastatic pancreatic cancer. Cancer Biol Ther **19**, 249–253, doi:10.1080/15384047.2016.1210743 (2018).
16. Jezek, P. 2-Hydroxyglutarate in Cancer Cells. Antioxid Redox Signal **33**, 903–926, doi:10.1089/ars.2019.7902 (2020).
17. Toth, L. N., de Abreu, F. B. & Tafe, L. J. Non–small cell lung cancers with isocitrate dehydrogenase 1 or 2 (IDH1/2) mutations. Human Pathology **78**, 138–143 (2018).
18. Nobusawa, S., Watanabe, T., Kleihues, P. & Ohgaki, H. IDH1 mutations as molecular signature and predictive factor of secondary glioblastomas. Clin Cancer Res **15**, 6002–6007, doi:10.1158/1078-0432.CCR-09-0715 (2009).
19. Hartmann, C. *et al.* Patients with IDH1 wild type anaplastic astrocytomas exhibit worse prognosis than IDH1-mutated glioblastomas, and IDH1 mutation status accounts for the unfavorable prognostic effect of higher age: implications for classification of gliomas. Acta neuropathologica **120**, 707–718 (2010).
20. Karlstaedt, A. *et al.* Oncometabolite d-2-hydroxyglutarate impairs alpha-ketoglutarate dehydrogenase and contractile function in rodent heart. Proc Natl Acad Sci U S A **113**, 10436–10441, doi:10.1073/pnas.1601650113 (2016).

21. Aniort, J. *et al.* Muscle wasting in patients with end-stage renal disease or early-stage lung cancer: common mechanisms at work. J Cachexia Sarcopenia Muscle **10**, 323–337, doi:10.1002/jcsm.12376 (2019).
22. Izquierdo-Garcia, J. L. *et al.* IDH1 Mutation Induces Reprogramming of Pyruvate Metabolism. Cancer Res **75**, 2999–3009, doi:10.1158/0008-5472.CAN-15-0840 (2015).
23. Zhou, Y. *et al.* Metascape provides a biologist-oriented resource for the analysis of systems-level datasets. Nature communications **10**, 1–10 (2019).
24. Neyroud, D. *et al.* FoxP1 is a transcriptional repressor associated with cancer cachexia that induces skeletal muscle wasting and weakness. J Cachexia Sarcopenia Muscle, doi:10.1002/jcsm.12666 (2021).
25. Leroy, C. *et al.* The 2q37-deletion syndrome: an update of the clinical spectrum including overweight, brachydactyly and behavioural features in 14 new patients. European Journal of Human Genetics **21**, 602–612 (2013).
26. Mohassel, P. *et al.* Anti-HMGCR myopathy may resemble limb-girdle muscular dystrophy. Neurology-Neuroimmunology Neuroinflammation **6** (2019).
27. Zheng, Q. *et al.* Systematic identification of genes involved in divergent skeletal muscle growth rates of broiler and layer chickens. BMC Genomics **10**, 87, doi:10.1186/1471-2164-10-87 (2009).
28. Kam, R. K. *et al.* Dhrs3 protein attenuates retinoic acid signaling and is required for early embryonic patterning. J Biol Chem **288**, 31477–31487, doi:10.1074/jbc.M113.514984 (2013).
29. Kim, H. S. & Lee, M. S. Frequencies of single nucleotide polymorphism in alcohol dehydrogenase7 gene in patients with multiple system atrophy and controls. Mov Disord **18**, 1065–1067, doi:10.1002/mds.10500 (2003).
30. Kunzke, T. *et al.* Derangements of amino acids in cachectic skeletal muscle are caused by mitochondrial dysfunction. J Cachexia Sarcopenia Muscle **11**, 226–240, doi:10.1002/jcsm.12498 (2020).
31. Popovici-Muller, J. *et al.* Discovery of AG-120 (Ivosidenib): a first-in-class mutant IDH1 inhibitor for the treatment of IDH1 mutant cancers. ACS medicinal chemistry letters **9**, 300–305 (2018).
32. Sulkowski, P. *et al.* Oncometabolites suppress DNA repair by disrupting local chromatin signalling. Nature **582**, 586–591, doi:10.1038/s41586-020-2363-0 (2020).
33. Boerner, T. *et al.* Genetic Determinants of Outcome in Intrahepatic Cholangiocarcinoma. Hepatology (2021).
34. Xin, M. *et al.* A threshold of GATA4 and GATA6 expression is required for cardiovascular development. *Proceedings of the National Academy of Sciences* **103**, 11189-11194 (2006).
35. Yadava, R. S. *et al.* RNA toxicity in myotonic muscular dystrophy induces NKX2-5 expression. Nature genetics **40**, 61–68 (2008).
36. Anderson, S. B., Goldberg, A. L. & Whitman, M. Identification of a novel pool of extracellular pro-myostatin in skeletal muscle. Journal of Biological Chemistry **283**, 7027–7035 (2008).

37. Blondet, B., Carpentier, G., Ferry, A. & Courty, J. Exogenous pleiotrophin applied to lesioned nerve impairs muscle reinnervation. Neurochemical research **31**, 907–913 (2006).
38. Chang, J. S. & Kong, I. D. Irisin prevents dexamethasone-induced atrophy in C2C12 myotubes. Pflugers Arch **472**, 495–502, doi:10.1007/s00424-020-02367-4 (2020).
39. Wijler, L. A. *et al.* Specialized nutrition improves muscle function and physical activity without affecting chemotherapy efficacy in C26 tumour-bearing mice. Journal of cachexia, sarcopenia and muscle **12**, 796–810 (2021).

Figures

Figure 1

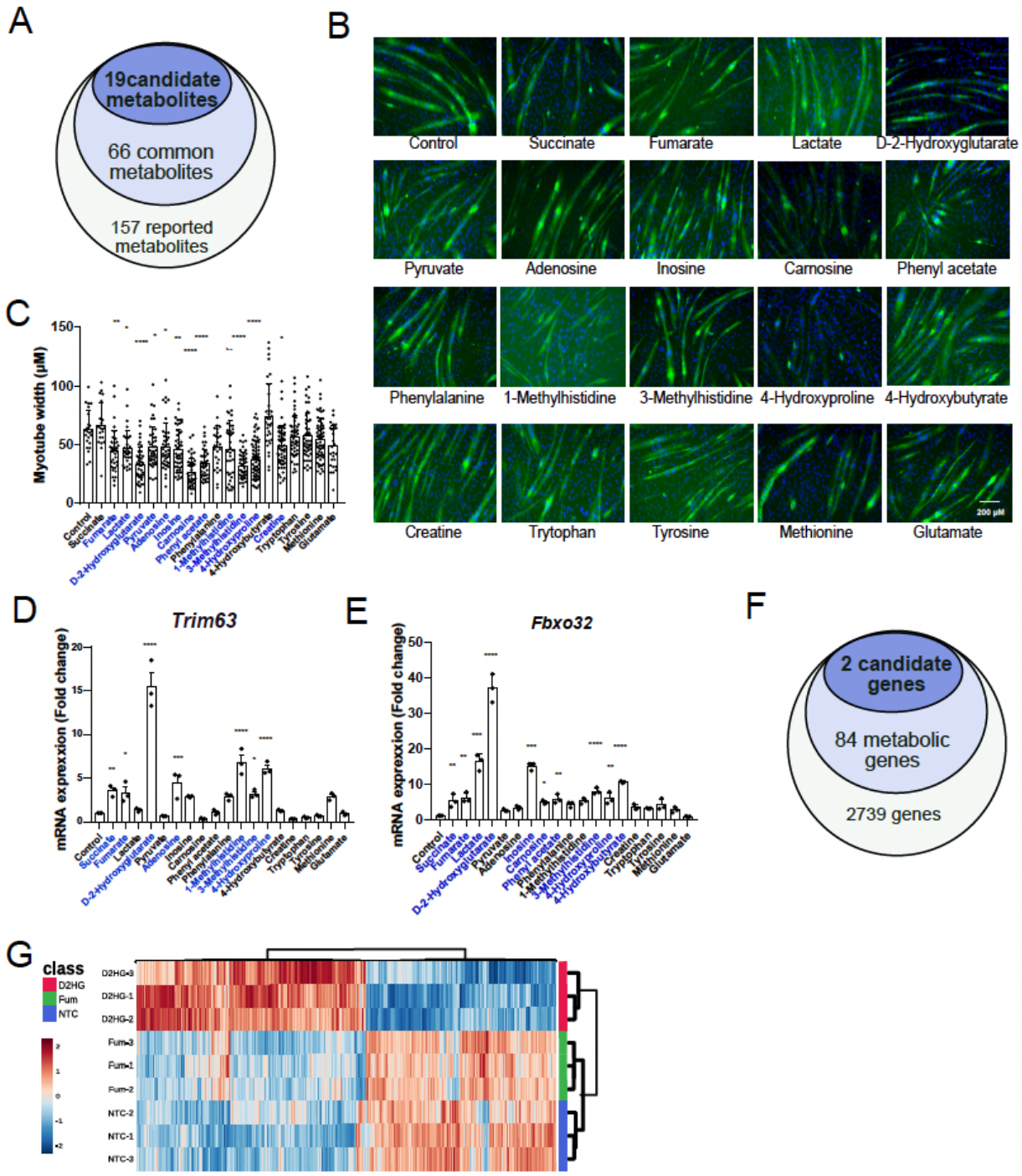

Figure 1

Screening of cachexia-related metabolites and identification of metabolites that induced muscle wasting. (A) Flowchart of the multi-tier selection of candidate metabolites related to muscle wasting. (B) Typical immunofluorescence morphological changes after metabolite treatments. Blue indicates DAPI, and green indicates MyHC (Scale bar: 100 μm). (C) Myotube diameter differences between different metabolite treatments. One-way ANOVA with post hoc Tukey's multiple-comparison test (****p<1e-4, ***p<2e-4,

p<2e-3, *p<0.033). Identification of metabolites that induce high expression of the E3 ligase *Trim63* (D) and *Fbxo32* (E). One-way ANOVA with post hoc Tukey's multiple-comparison test (**p<1e-4, ***p<2e-4, **p<2e-3, *p<0.033). (F) Screening of common genes related to altered cancer based on a Venn diagram. (G) Heatmap of differentially expressed genes after D2HG and Fum treatment of well-differentiated myotubes relative to NTC myotubes. Each group was tested in triplicates. Gene expression values were given as fragments per kilobase per million.

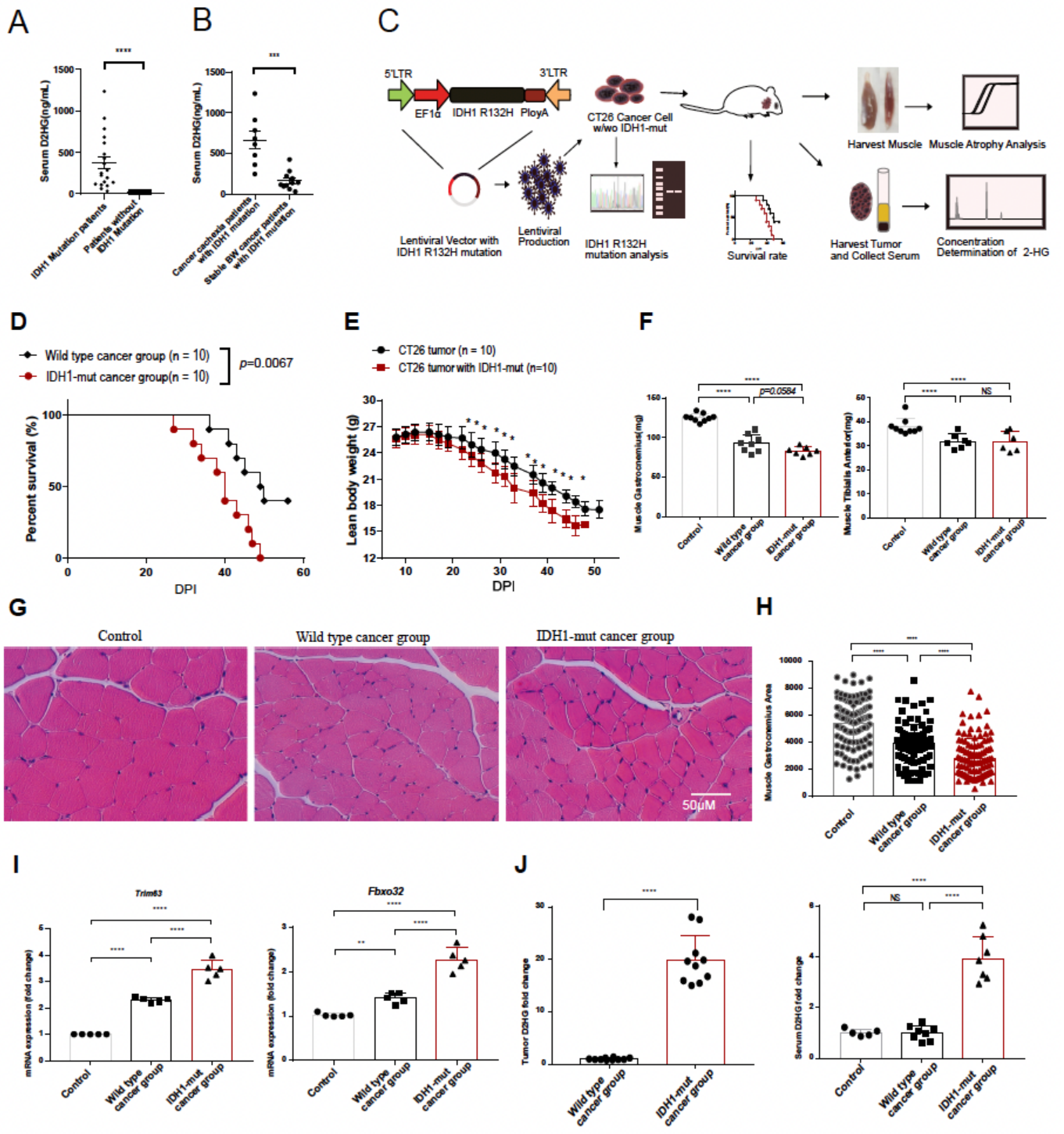

Figure 2

IDH1 mutation-mediated D2HG accumulation in cancer patients and *in vivo*. (A) Column plot of serum D2GH levels in 194 cancer patients with/without IDH1 mutation. Unpaired two-tailed t-test (****p<1e-4, ***p<2e-4, **p<2e-3, *p<0.033). (B) Column plot of serum D2GH levels in cancer cachexia patients with an IDH1 mutation and stable body weight cancer patients with an IDH1 mutation. Unpaired two-tailed t-test (****p<1e-4, ***p<2e-4, **p<2e-3, *p<0.033). (C) Schematic of the i*n vivo* experiment design for IDH1

(R132H) mutation in CT26 tumor-induced skeletal muscle atrophy and cancer cachexia syndrome. (D) Survival curve of mice with IDH1 (R132H) mutated cancer and wild-type cancer. Log-rank (Mantel-Cox) test (****p<1e-4, ***p<2e-4, **p<2e-3, *p<0.033). (E) Tumor weight of IDH1 (R132H) mutated cancer and wild-type cancer. Unpaired two-tailed t-test (*p<0.05). (F) The lean body weight (=whole body weight-tumor weight) of the IDH1 (R132H) mutated cancer and wild-type cancer groups. Unpaired two-tailed t-test. (*p<0.05 IDH1 (R132H) mutated cancer vs. wild type cancer. #, p<0.05 wild-type cancer vs. and normal control). (G) Column plot of the muscle gastrocnemius and anterior tibial muscle in IDH1 (R132H) mutated cancer-bearing mice and wild-type cancer-bearing mice. One-way ANOVA with post hoc Tukey's multiple-comparison test (****p<1e-4, ***p<2e-4, **p<2e-3, *p<0.033). (H) Column plot of mRNA expression of *Fbxo32* and *Trim63* in IDH1 mutated cancer-bearing mice and wild-type cancer-bearing mice. One-way ANOVA with post hoc Tukey's multiple-comparison test (****p<1e-4, ***p<2e-4, **p<2e-3, *p<0.033). (I) Typical cross-section histopathological image of the muscle gastrocnemius (Scale bar: 50μm). (J) Column plot of the cross-section area of muscle gastrocnemius in IDH1 mutated cancer-bearing mice and wild-type cancer-bearing mice. One-way ANOVA with post hoc Tukey's multiple-comparison test (****p<1e-4, ***p<2e-4, **p<2e-3, *p<0.033). (K) Column plot of tumor and serum D2HG levels in IDH1 mutated cancer-bearing group and wild-type cancer-bearing mice. One-way ANOVA with post hoc Tukey's multiple-comparison test (****p<1e-4, ***p<2e-4, **p<2e-3, *p<0.033).

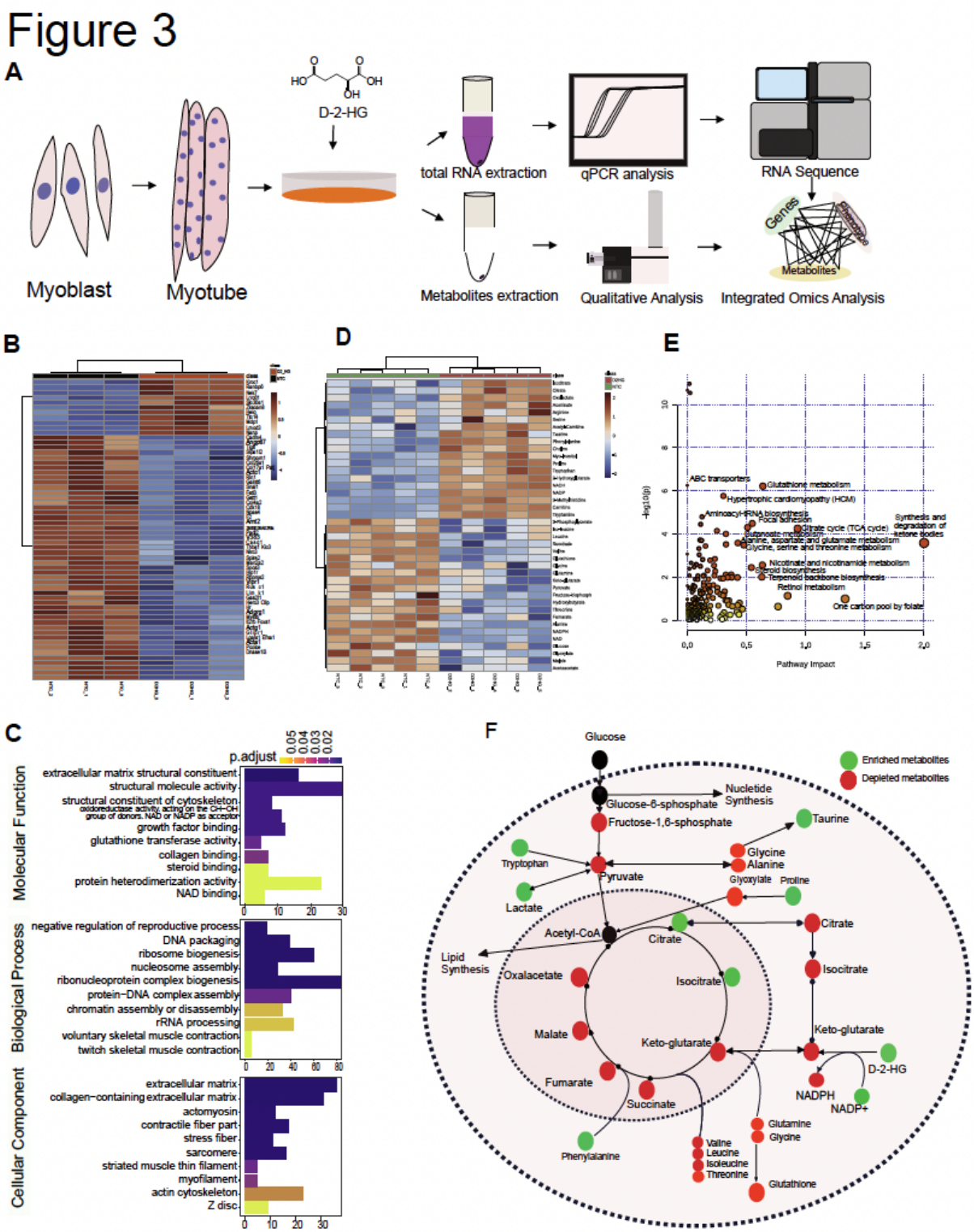

Figure 3

D2HG induces muscle wasting through activation of UPP and metabolic reprogramming of the hydroxy compound biosynthetic process. (A) Schematic of the *ex vivo* experiment designed to determine whether D2HG directly induces muscle atrophy. (B) Heatmap of differentially expressed genes in D2HG-treated well-differentiated myotubes relative to NTC myotubes. All experiments were performed in triplicate. Gene expression values were given as the fragments per kilobase per million. (C) GO enrichment analysis of

D2HG versus control well-differentiated myotubes. (D) Heatmap of the relative abundance of differential metabolites between D2HG-treated well-differentiated myotubes and NTC myotubes. Each group had five replicates. (E) Integrated analysis of transcriptome profiling and metabolomics profiling revealed the significantly changed pathway resulted from D2HG. (F) Summary illustration highlighting metabolites on simplified metabolic pathways adapted from the KEGG metabolic pathways. Red circles indicate decreased metabolites; blue circles indicate increased metabolites.

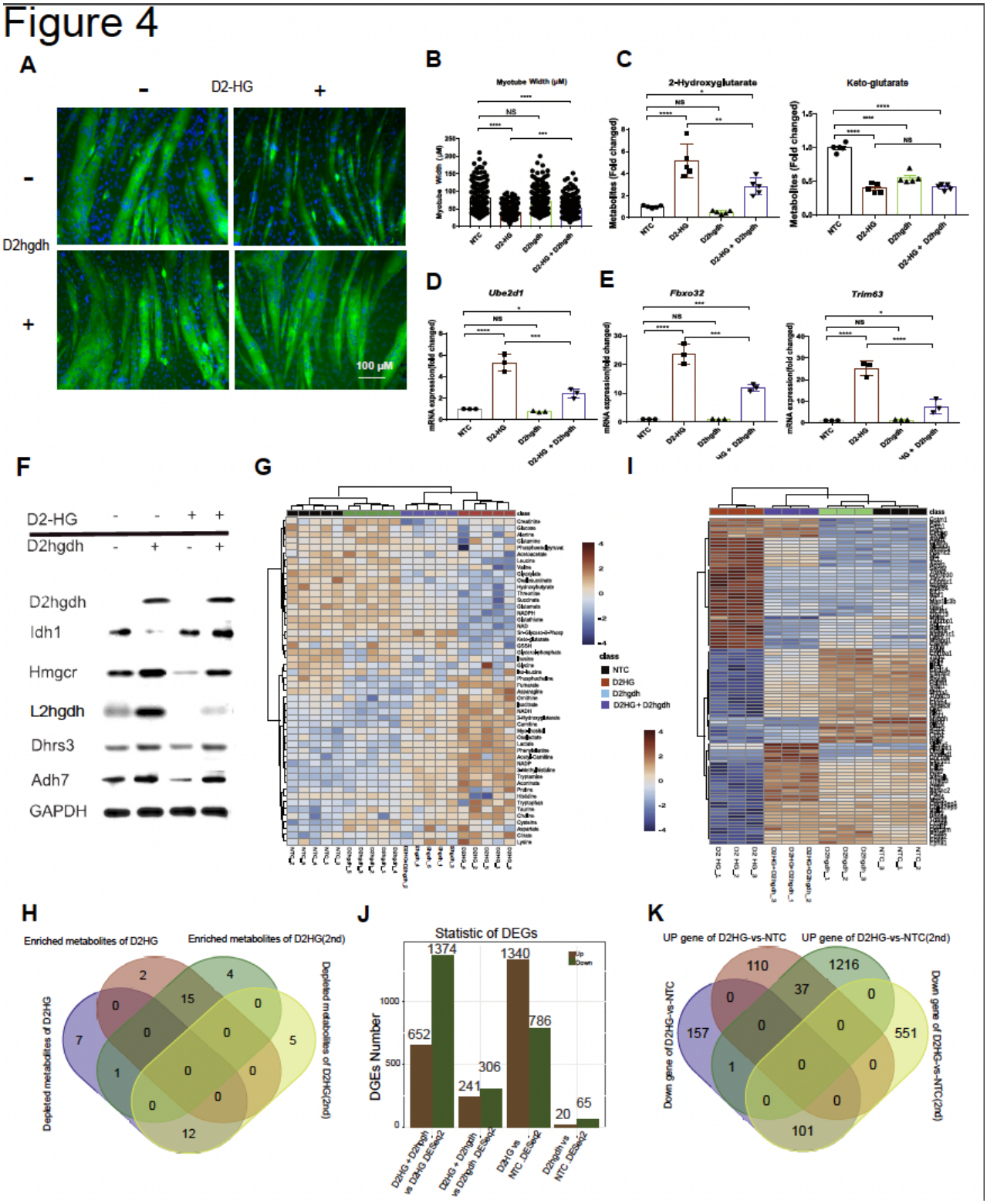

Figure 4

D2hgdh reversed D2HG-induced muscle wasting by inhibiting the UPP-mediated proteolysis and metabolic reprogramming. (A) Typical immunofluorescence morphological changes of D2hgdh overexpressing and NTC myotubes after metabolites D2HG treatment (Scale bar: 100μm). (B) Column plot of myotube width in NTC and D2HG-treated well-differentiated myotubes with/out D2hgdh overexpression. One-way ANOVA with post hoc Tukey's multiple-comparison test (****p<1e-4, ***p<2e-4,

p<2e-3, *p<0.033). (C) Column plot of metabolites changes in NTC and D2HG-treated well-differentiated myotubes with/out D2hgdh overexpression. One-way ANOVA with post hoc Tukey's multiple-comparison test (**p<1e-4, ***p<2e-4, **p<2e-3, *p<0.033). (D-E) Column plot of mRNA expression of *Ube2d1, Trim63* and *Fbxo32* in NTC and D2HG-treatedwell-differentiated myotubes with/out D2hgdh over-expression. One-way ANOVA with post hoc Tukey's multiple-comparison test (****p<1e-4, ***p<2e-4, **p<2e-3, *p<0.033). (F) Western blot results of protein expression in NTC and D2HG-treated well-differentiated myotubes with/out D2hgdh overexpression. GAPDH was used as an internal reference. (G) Heatmap of relative abundance of differential metabolites in NTC and D2HG-treated well-differentiated myotubes with/out D2hgdh overexpression. Each group had five replicates. (H) Venn diagram showing commonly changed metabolites resulting from D2HG treatment. (I) Heatmap of differentially expressed genes in NTC and D2HG-treated well-differentiated myotubes with/out D2hgdh overexpression. Each group had three replicates. (J) Summary of differently expressed genes in NTC and D2HG treated well-differentiated myotubes with/out D2hgdh overexpression. (K) Venn diagram showing commonly changed genes resulting from D2HG treatment.

Figure 5

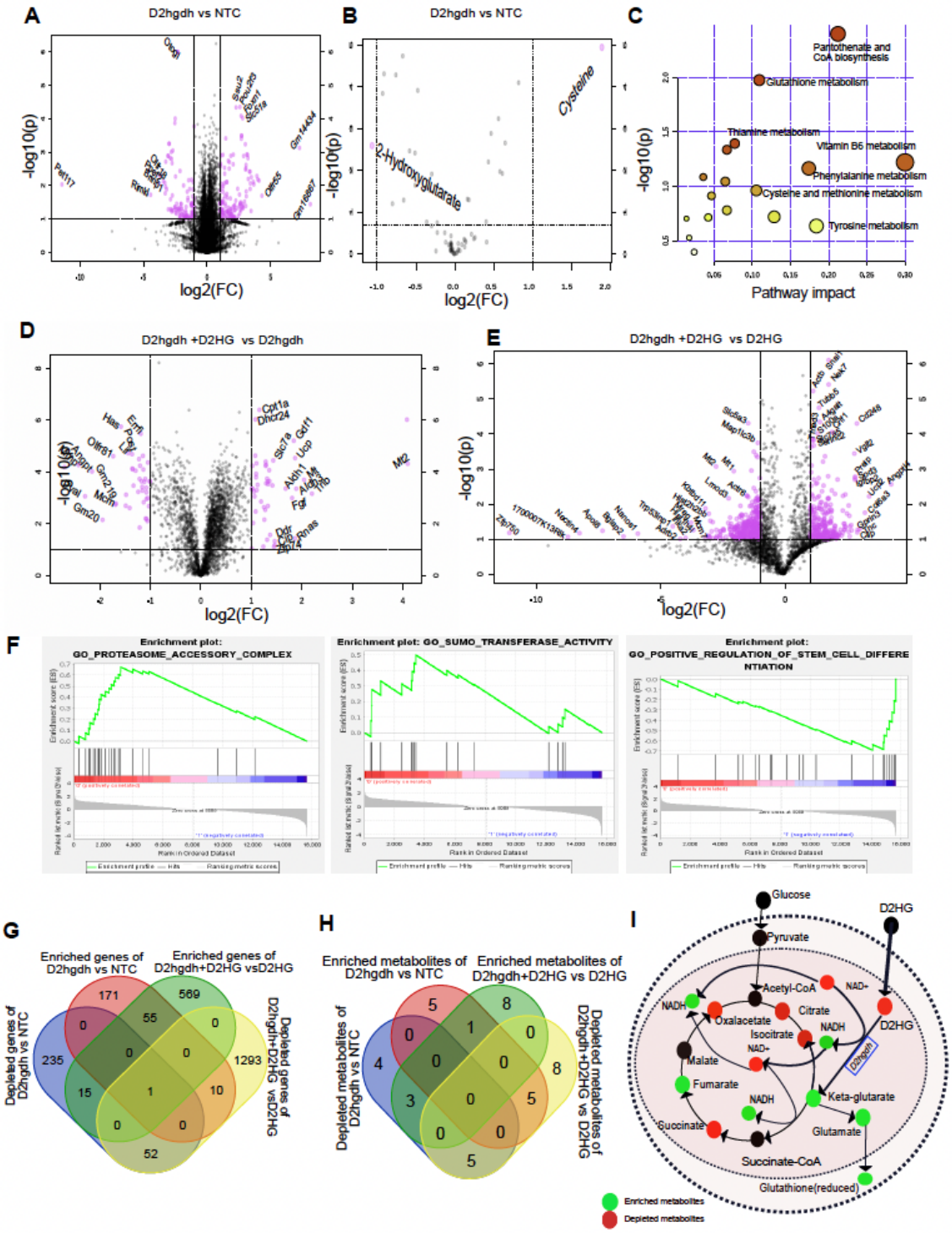

Figure 5

D2hgdh reversed D2HG-induced muscle wasting through metabolic reprogramming. (A) Volcano plot showing the significantly changed genes between the D2hgdh overexpression and NTC groups. Significance was defined as fold change 2.0 and p<0.05. (B) Volcano plot showing the significantly changed metabolites between the D2hgdh over-expression and NTC groups. Significance was defined as fold change 2.0 and p<0.05. (C) Integrated analysis of transcriptome profiling and metabolomics profiling

revealing the significantly changed pathway resulting from D2hgdh overexpression. (D) Volcano plot showing the significantly changed genes between D2HG-treated D2hgdh overexpression myotubes and negative treated D2hgdh overexpression myotubes. Significance was defined as fold change 2.0 and p<0.05. (E) Volcano plot showing the changed genes between D2HG-treated D2hgdh overexpressing myotubes and D2HG-treated control myotubes. Significance was defined as fold change 2.0 and p<0.05. (F) Gene Set Enrichment Analysis of altered pathway resulted from D2HG. (G) Venn diagram showing commonly changed genes resulting from D2hgdh over-expression. (H) Venn diagram showing the commonly changed metabolites resulting from over-expression. (I) Column plot of NADH/NAD ratio and NADPH/NADP in the four groups. One-way ANOVA with post hoc Tukey's multiple-comparison test (****p<1e-4, ***p<2e-4, **p<2e-3, *p<0.033). (J) Summary illustration of metabolites on a simplified metabolic pathway adapted from KEGG metabolic pathways. Red circles indicate decreased metabolites; blue circles indicate increased metabolites.

Figure 6

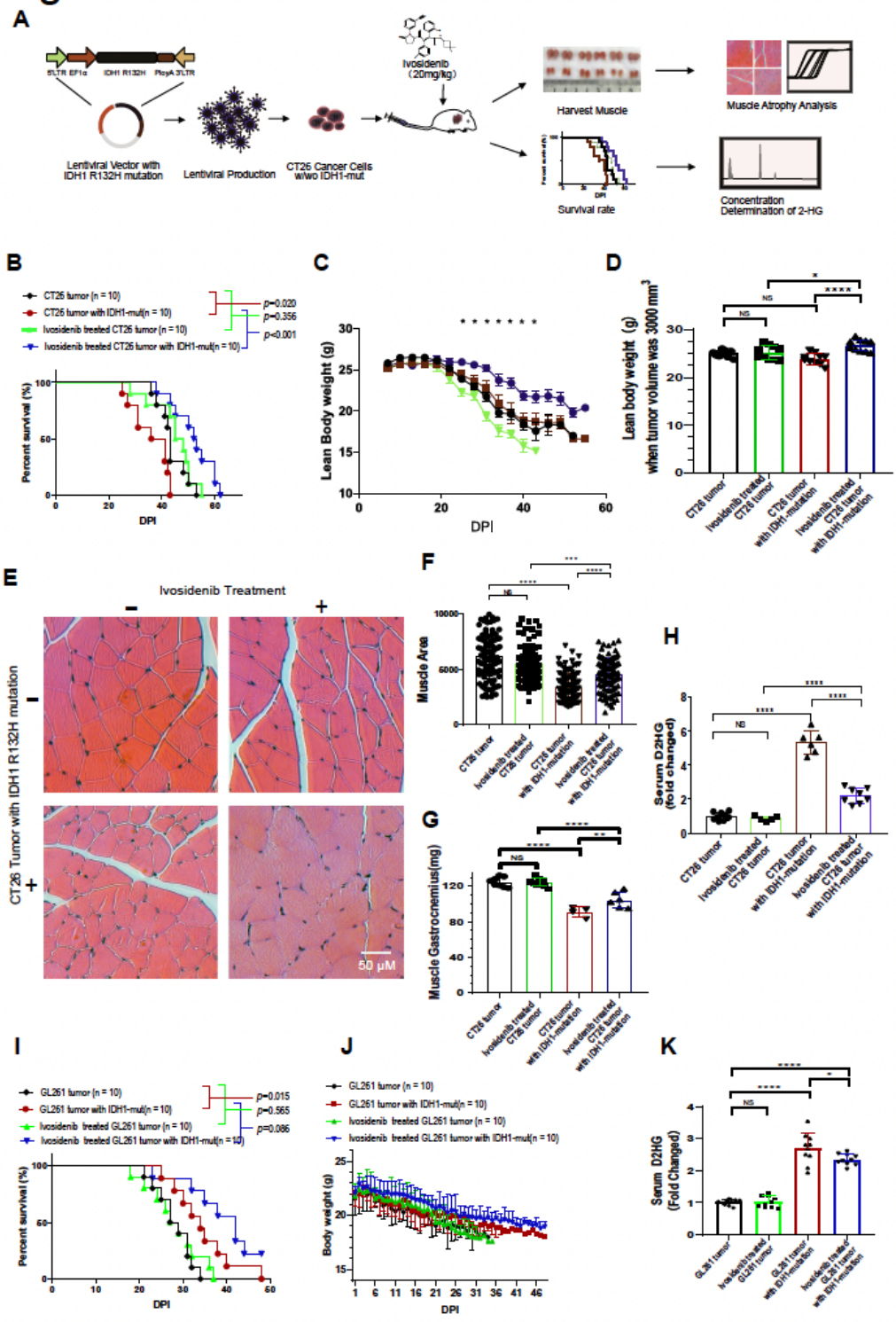

Figure 6

Ivosidenib ameliorates IDH1 mutation-mediated skeletal muscle atrophy and inhibits the accumulation of serum D2HG. (A) Schematic of the *in vivo* experiment. (B) The survival curve of IDH1 (R132H) mutation cancer and wild-type cancer groups treated with ivosidenib or NTC. Log-rank (Mantel-Cox) test. (C) The lean body weight of mice in the IDH1 (R132H) mutational cancer group and wild-type cancer group treated with ivosidenib or NTC. ANOVA following Tukey's multiple comparisons test; the lean body weight

difference between ivosidenib treated mice bearing IDH1 mutation tumor vs. NTC treated mice bearing IDH1 mutation tumor was significant (*p<0.05). (D) Mice with a similar tumor weight of 3000 mm^3 (1.56g), the lean body weight was compared in IDH1-R132H and IDH1wt cancer treated with ivosidenib or NTC. One-way ANOVA with post hoc Tukey's multiple-comparison test (****p<1e-4, ***p<2e-4, **p<2e-3, *p<0.033). (E) Typical cross-section histopathological image of muscle gastrocnemius in IDH1 (R132H) mutational cancer and wild type cancer treated with ivosidenib or NTC (Scale bar: 50μm). (F) Column plot of the cross-section area of muscle gastrocnemius in IDH1 (R132H) mutation cancer and wild-type cancer treated with ivosidenib or NTC. One-way ANOVA with post hoc Tukey's multiple-comparison test (****p<1e-4, ***p<2e-4, **p<2e-3, *p<0.033). (G) Column plot of muscle gastrocnemius weight in IDH1-R132H and IDH1wt cancer treated with ivosidenib or NTC. One-way ANOVA with post hoc Tukey's multiple-comparison test (****p<1e-4, ***p<2e-4, **p<2e-3, *p<0.033). (H) Column plot of serum D2HG concentration in IDH1 (R132H) mutational cancer group and wild type cancer group treated with ivosidenib or NTC. One-way ANOVA with post hoc Tukey's multiple-comparison test (****p<1e-4, ***p<2e-4, **p<2e-3, *p<0.033). (I) The survival curve of IDH1 (R132H) mutation cancer and wild-type cancer groups treated with ivosidenib or NTC. Log-rank (Mantel-Cox) test. (J) The body weight of mice in the IDH1 (R132H) mutational GL261 tumor group and wild-type GL261 tumor group treated with ivosidenib or NTC. (K) Column plot of serum D2HG concentration in IDH1 (R132H) mutational GL261 cancer group and wild type GL261 cancer group treated with ivosidenib or NTC. One-way ANOVA with post hoc Tukey's multiple-comparison test (****p<1e-4, ***p<2e-4, **p<2e-3, *p<0.033).

Figure 7

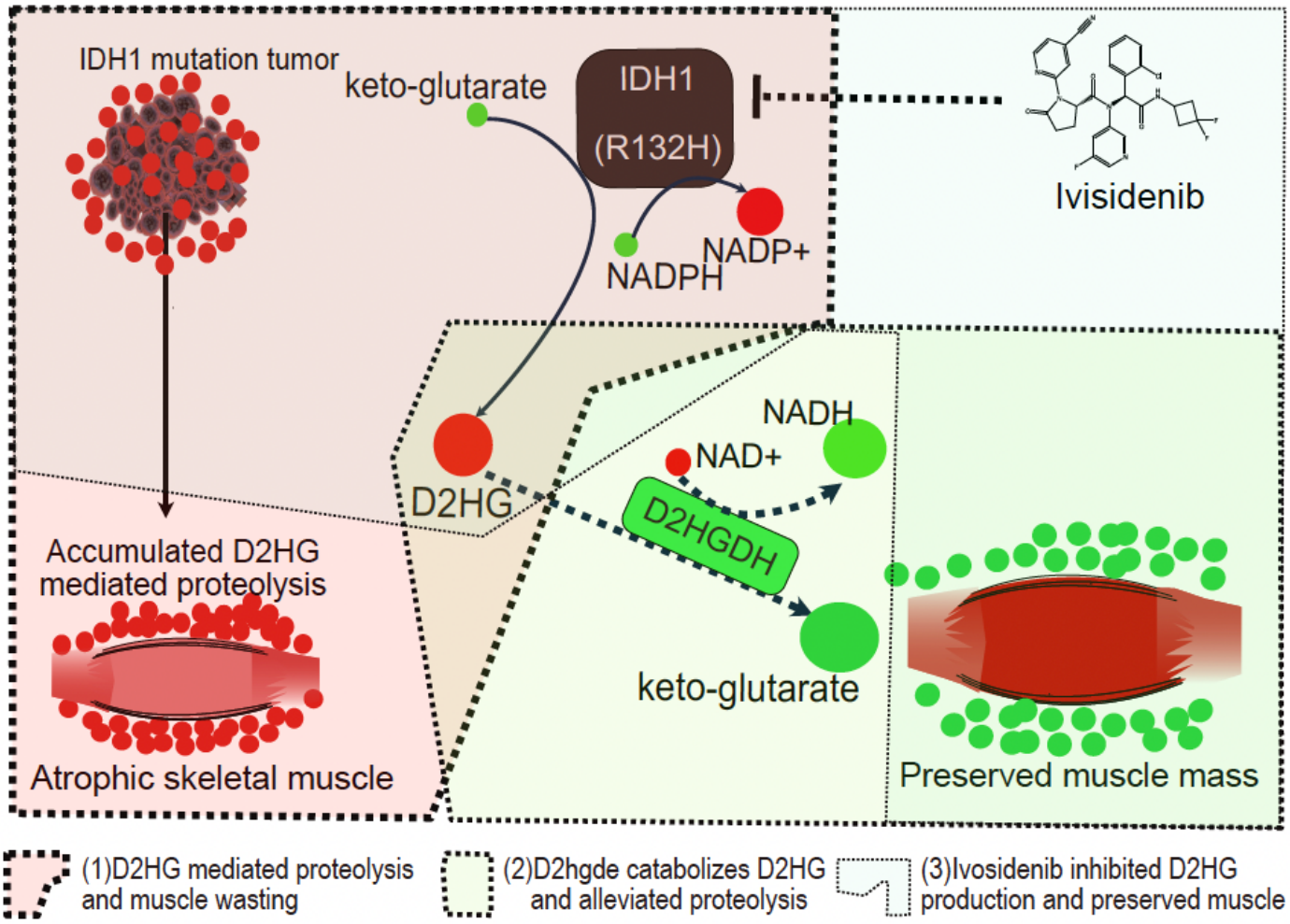

Figure 7

The metabolic scheme of IDH1 mediated D2HG accumulation and its contribution of proteolysis and muscle wasting. The accumulated D2HG can be catabolized by enzyme D2HGDH and the production of D2HG can be inhibited by IDH1 inhibitor ivosidenib.

Supplementary Files

This is a list of supplementary files associated with this preprint. Click to download.

- Supplementarymaterials.docx
- SupMeta.pdf
- TableS1Cancercachexiarelatedmetabolites.xls
- TableS2Candidatemetabolitesandtheconcerntration.xlsx

- TableS3Alteredgenesofcancer.xlsx
- TableS4Metabolismrelatedoncogene.xlsx
- TableS5cancerandcancerpatients2.xls
- TableS6D2HGinducedmetabolitesalteration.xls
- TableS7.xls
- TableS8.xls
- TableS9.xls
- TableS10.xls
- TableS11.xls
- TableS12.xls
- TableS13.xls
- TableS14.xls
- TableS152.xls
- TableS16.xlsx